EFFECTS OF CORIOLIS ON TURBULENT FLOW IN ROTATING RECTANGULAR CHANNELS

by

JOHN MOORE
B.Sc. (Eng.), Imperial College, London University,
(1965)

Submitted in Partial Fulfillment of the
Requirements for the Degree of
Master of Science
in
Mechanical Engineering
at the
Massachusetts Institute of Technology
January 1967

Signature of Author _____
Department of Mechanical Engineering

Certified by _____
Thesis Supervisor

Accepted by _____
Chairman, Departmental Committee on Graduate Studies

EFFECTS OF CORIOLIS ON TURBULENT FLOW IN ROTATING RECTANGULAR CHANNELS

by

JOHN MOORE

Submitted to the Department of Mechanical Engineering on January 16, 1967, in partial fulfillment of the requirements for the Degree of Master of Science in Mechanical Engineering.

ABSTRACT

An experimental and theoretical study has been made of fully developed turbulent flow in rotating, rectangular radial-flow channels. The transverse pressure gradient associated with the Coriolis acceleration of fluid flowing in rotating channels can interact with the velocity profile to produce secondary circulations, and to alter transverse velocity fluctuations and momentum transfer. The relative importance of these two effects is studied experimentally in rectangular channels of different aspect ratios (height, L/width, D). Rotational effects are seen to depend on the Reynolds' number ($\rho U d_h/\mu$), a spin parameter $\omega D/U$ and the aspect ratio L/D.

Measurements of velocity profiles, wall shear stresses and u' turbulence distributions are made for spin rates up to $\omega D/U = 0.08$. Relatively large effects are measured at the 1/2:1 and 1:1 aspect ratios while much smaller effects are noticed in the 4:1 and 7 1/3:1 ducts. Indeed, the experimental measurements suggest that secondary circulations provide the mechanism for the most important rotational effects in the present range of spin parameter.

A Second Order solution of the Navier-Stokes equations used by Barua to calculate the perturbation effects of rotation on fully developed laminar flow in a circular pipe is modified to apply approximately to turbulent flow in rectangular channels. Within the limitations of low spin rate and an uncertainty as to the eddy viscosity, it is found possible to calculate the rotational effects on the centerline velocity profile quite closely, and a better understanding of the flow is gained. The calculation omits any effects of Coriolis instability.

The change in friction factor is measured and compared with the predictions, based on data for bent circular pipes, of a useful analogy between the flow in rotating, bent and heated horizontal channels. The predictions are seen to show reasonable agreement with the data obtained for the square channel.

Thesis Supervisor _____

Title: Associate Professor of Mechanical Engineering

ACKNOWLEDGEMENTS

The author wishes to express his gratitude to Professor Philip G. Hill, thesis supervisor, for his guidance and encouragement throughout the project, and to Professor Edward S. Taylor, Director of the Gas Turbine Laboratory, whose interest and insight were greatly valued. He is indebted to Professor Hal L. Moses for many stimulating discussions and to Dr. Brian E. Launder who initiated the present work and introduced the author to the problems involved.

Credit for the initial construction of the apparatus must go to Mr. I-Man Moon, while the skillful assistance and advice of Mr. Thorvald Christensen were much appreciated in performing those modifications necessary to complete the present tests. The numerical calculations were performed with the assistance of the Massachusetts Institute of Technology Computation Center, and here the author is especially grateful to Mrs. Joan Kukolich for ably programming the theoretical computations. Mrs. Madelyn M. Euvrard endeared herself to the author by many thoughtful kindnesses, and he is most grateful to her and Mrs. Gillian Benton for typing the manuscript.

The project was made possible by the National Science Foundation under Grant No. 74922.

TABLE OF CONTENTS

NOMENCLATURE

A.R.		Aspect Ratio = $\frac{L}{D}$
B_k		Constant in "Slip velocity" boundary condition
C		Dimensionless axial static pressure gradient
d_h		Hydraulic diameter
D		Channel width
f		Friction factor
f_c, f_R, f_s		Friction factors for curved, rotating and straight ducts
$\frac{i}{x}, \frac{j}{y}, \frac{k}{z}$		Coordinates and coordinate directions (see Fig.2)
K	=	$\frac{2\omega D^3 U}{\nu^2}$ parameter of rotating flow
L		Channel height
n		Outward radius of curved duct
n_o		Radius of curved duct
N		Radius of curvature of curved duct
p		Static pressure
R	=	R_e/R_o
R_{e_L}		$\frac{\rho \bar{U} d_h}{\mu}$; $R_{e_T} = \frac{\rho \bar{U}}{\nu}$
R_e		Reynolds' Number (Laminar or turbulent) based on uniform viscosity
R_o	=	$\frac{U}{2\omega D}$ = Rossby Number
u,v,ω		Total velocity component
u_τ	=	$\sqrt{\tau_o/\rho}$ friction velocity
U		Peak no-rotational velocity
U_R		Peak rotational velocity

$\overline{U}$	Bulk mean velocity
V	Vector Representation of complete velocity
Δp	Pressure drop
Δ_{sub}	Sublayer thickness
μ	Molecular viscosity
ν	Eddy viscosity
ξ	Momentum parameter
ρ	Density
τ_o	Wall shear stress
ψ	Stream function in y-z plane
ω	Angular velocity

LIST OF FIGURES

I. INTRODUCTION

One of the major problems in designing centrifugal compressors is the accurate prediction of impeller-exit/diffuser-entry flow conditions. The flow in the impeller is affected by an interaction between the transverse pressure gradient, arising from the Coriolis acceleration, and the wall boundary layers. This interaction may cause major modifications to the exit velocity profile which can in turn influence the flow in the diffuser, thereby affecting the overall performance of the machine.

Interactions between transverse pressure gradients and wall boundary layers also occur in bent channels and heat horizontal ducts, and it may be expected that the three flow patterns will be similar since there is an unbalanced body force in each case. The similarity is approximate and it is immediately apparent for example that the Coriolis forces in rotating tubes are proportional to the velocity, while centrifugal forces in bent tubes vary as the square of the velocity. Trefethen[1,2] has shown however that the friction factor variations due to the secondary flow patterns in the three cases can be expressed in terms of the Reynolds Number (R_{e_L}) of the flow and a dimensionless group characterizing each of the three cases. This dimensionless group when properly specified provides a quantitative connection between flows.

In specifying the parameters which determine the friction factor (and heat transfer) changes Trefethen assumes that "with the diameter, total flow, and viscosity fixed, the flow pattern in a long tube is determined solely by the difference in transverse body force per unit volume between the fluid at the wall and fluid at the average velocity and average temperature". The differences in transverse body forces thus

obtained are:

$$\frac{\rho\bar{U}^2}{N} \ , \ 2\rho\bar{U}\omega \quad \text{and} \quad \rho g\beta(T_m - T_w)$$

for the bent, rotating and heated pipes, respectively, and the corresponding parameters are:

$$R_{e_L}\sqrt{n_o/N}, \ R_{e_L}\sqrt{2\omega n_o/\bar{U}} \ , \ \sqrt{\rho g\beta(T_m - T_w)\ (8n_o^3)/2\mu^2}$$

A subsequent comparison of friction factors and heat transfer coefficients for laminar flow in tubes, and friction factors for turbulent flow in tubes, led to the conclusion that the secondary flows are similar if the force differences are of the same size. Also it was found that the **critical** Reynolds Number for transition between laminar and turbulent flow is similarly increased by bending and rotation. Although the analogy is not strictly applicable in every detail it provides a good platform from which to view the phenomena considered throughout this report and also suggests possible extensions of the general conclusions.

There are two possible mechanisms by which Coriolis acceleration can affect the turbulent boundary layer, Coriolis instability and secondary flows.

A. Coriolis Instability

It has been found by Liepmann[3], Eskinazi and Yeh[4] and Margiolis and Lumley[5] (among many others) that for flow in a curved duct the boundary layer fluid on the concave wall is considerably more unstable

and transition occurs more readily on this surface than on the convex wall. Consideration of the flow of an inviscid fluid between co-axial cylindrical walls led Rayleigh[6] and Prandtl[7] to an inviscid stability criterion based on the stability of a fluid particle in the transverse centrifugal pressure gradient. The criterion for stable motion being

$$\frac{\partial(ru)}{\partial r} > 0$$

where r is the outward radius for the curved flow. This argument when applied to a rotating duct with the transverse centrifugal pressure gradient replaced by the Coriolis pressure gradient proceeds as follows:-

Consider a fluid particle in the boundary layer on the pressure side of the rotating duct (see sketch below). The motion of the particle normal to the pressure surface is governed, in the absence of shear forces, by the interaction between the Coriolis force experienced by this particle and the local transverse pressure gradient balancing the mean motion of all particles passing through that location.

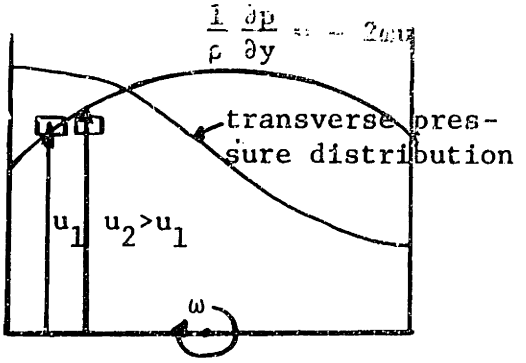

If the particle were displaced away from the wall without any significant change in its streamwise momentum component it would enter a region where the mean streamwise momentum and the associated local pressure gradient were larger. The new pressure forces would therefore exceed the Coriolis force and accelerate the particle further from the pressure surface. Similarly, a lateral movement toward the pressure surface would be furthered rather than opposed by the local

pressure gradient, and the particle motion is seen to be unstable. On the suction side of the duct the same reasoning can be used to show that turbulent fluctuations normal to the wall are opposed by the local transverse pressure gradient, and the particle motion is stable. Recent measurements by Halleen[8] have shown that Coriolis instability effects can be significant and are qualitatively as predicted by this argument which results in the criterion for stability as $\partial u/\partial y > 0$.

The conclusion drawn from the above argument is that Coriolis forces should tend to increase the turbulent momentum exchange in the boundary layer on the pressure side of the channel and inhibit it on the suction side. Thus the velocity profile could be modified to show a thinner boundary layer on the pressure side.

B. Secondary Flows

Thomson[9] in an explanation of the deposition of detritus on the inner banks of river bends recognized the existence of a layer of fluid near the bottom of the river which is retarded by viscous action. He argued that this layer moves towards the inner bank under the influence of the centrifugal pressure gradient set up by the curvature of the faster moving stream above it. Further, he demonstrated these secondary flows in a curved water channel using threads and small particles which moved with the fluid[10].

The rotating rectangular channels considered by Hill and Moon[11] and Moon[12], and the impeller of a centrifugal compressor provide analogous examples of this situation in which the Coriolis pressure gradient set up by the primary flow influences the top and bottom wall (hub and shroud)

boundary layers. The boundary layer fluid is then convected towards the suction surface (see sketch below) while retaining its axial momentum , and there arises the possibility of secondary flow circulations. (It should be noted however that these examples also provide the possibility of Coriolis instability). In fully developed flow there are, strictly speaking, no boundary layers but a corresponding imbalance between the Coriolis and pressure forces acting on the "slow-moving particles" near the top and bottom walls of the channel can cause similar secondary flows.

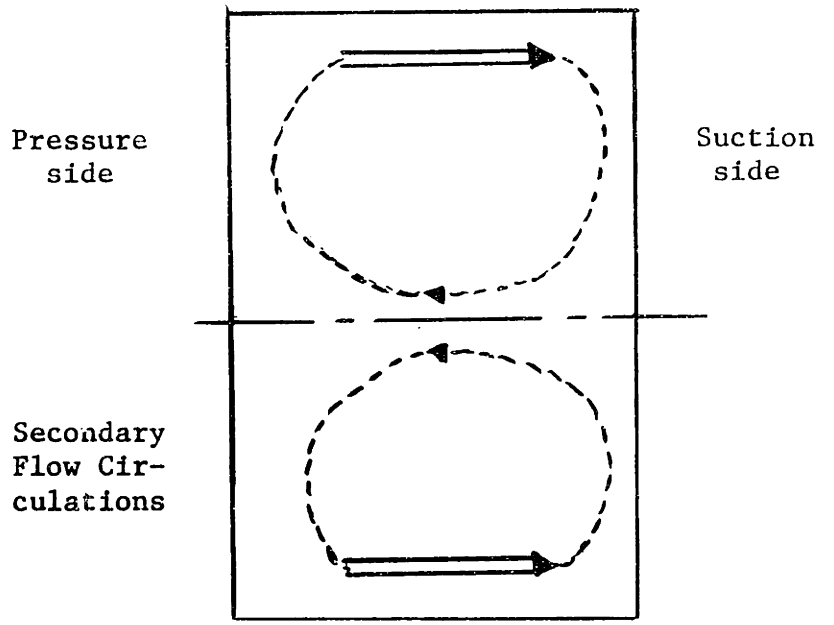

The experimental results of references (11) and (12) showed that rotational effects can be large and significant on the development of a turbulent boundary layer in a rotating rectangular channel. In particular the wall shear stress on the pressure surface was higher than for a zero pressure gradient boundary layer, while on the suction side it was lower. Also the developing velocity profiles obtained by Moon[12] show striking resemblance to the mid-passage profiles measured by Lohmann[13] in his

investigation of the exit planes of several impeller configurations. Indeed Lohmann has concluded the existence of an accumulation of low relative-momentum fluid on the suction surface of his test impellers as the direct result of secondary flows.

Most of the effects of rotation observed by Moon on the shape of the velocity profiles and on the wall shear stresses could be explained by either of the mechanisms. The higher shear stress on the pressure side could equally well be due to increased turbulent momentum exchange or to the removal of low momentum boundary layer fluid by secondary circulations. Similarly the lower shear stress on the suction side could be caused by secondary flow depositions or reduced momentum exchange. Hence, at the "centerline" of the duct it is possible, in principle, to separate the effects of secondary flows from those due to Coriolis instability.

In the present study it was decided to try to determine the relative importance of these two effects in fully-developed flow in rectangular ducts of varying aspect ratio (height/width). An increase in the height of a constant-width duct effectively moves the driving force of the secondary flow away from the duct centerline, while maintaining an approximately constant transverse pressure gradient.

Experimental investigations were performed in rectangular channels of aspect ratios 1/2:1, 1:1, 4:1 and 7 1/3:1 to determine the effects of spin rates up to $\omega D/\bar{U} = 0.08$ on the centerline flow. Axial velocity profiles, wall shear stresses and u' turbulence distributions as well as axial static pressure drops were measured for the fully-developed flow. Relatively large effects were measured at the 1/2:1 and 1:1 aspect ratios while much smaller effects were noticed in the 4:1 and 7 1/3:1 ducts.

Indeed the experimental measurements suggested that secondary circulations provide the mechanism for the most important rotational effects in the present range of spin parameter. Although these circulations involve very small velocities in the plane normal to the axial direction changes in axial velocity of up to 20% and in shear stress of up to 50% were recorded at the small aspect ratios.

The relative importance of secondary flows shown by the experiments led to an attempt to calculate the secondary axial velocities. This was based on a linearized First Order theory used by Benton[14] to predict the effects of Coriolis acceleration on laminar flow in a long pipe, combined with a Second Order theory given by Dean[15] for the analogous flow in a bent pipe, and later modified by Barua[16] in his analysis of laminar flow in a rotating circular pipe. The analyses of both Benton and Barua are only applicable for low rotational speeds, while a more recent study by Boyer[17] only applies for arbitrarily large spin rates. Although the range of usefulness of Boyer's analysis is well away from the present experiments, it was found that a very approximate extension of Barua's theory could be applied to the lowest spin rates. The extension involved representing the turbulent flow in a rotating rectangular channel by flow with uniform isotropic eddy viscosity, connected to the wall by a region of constant shear stress which included a thin laminar "slip velocity" layer. The constant shear stress region led to a boundary condition of the form $u = B_k \frac{\partial u}{\partial y}$. Within the limitations of low spin rate and an uncertainty as to the eddy viscosity it was found possible to calculate the rotational effects on the centerline velocity profile quite closely, and a better understanding of the flow was gained. The calculation omitted any

effects of Coriolis instability.

Fully-developed turbulent flow in a rotating rectangular duct may be considered as governed by three parameters

$$R_{e_L} = \frac{\rho \bar{U} d_h}{\mu} , \frac{\omega D}{\bar{U}} \text{ and } \frac{L}{D} ,$$

the Reynolds number, a spin parameter and the aspect ratio. Actually the important ratio of forces is the Coriolis to the viscous but in a turbulent flow the shear stress obeys no simple relation as do Newtonian fluids. Also the Reynolds' normal stresses add further complexity absent in laminar flow. The eddy viscosity ν is often used in turbulent flows as a useful means of relating the shear stress to the mean velocity profile. Unlike the laminar kinematic viscosity it is not isotropic, nor a property of the fluid, but it has been found for two-dimensional turbulent boundary layers that the simple assumption $\nu/U\delta$ = constant gives reasonable results for the outer part of the boundary layer[18]. Indeed, a quite successful method for calculating the outer 80% of the boundary layer velocity profile is available using a similar assumption[19]. An extension of this assumption to give $2\nu/UD$ = constant seems one of the few ways of estimating ν for a rectangular duct. An order of magnitude analysis may then be used to obtain a typical ratio of

$$\frac{\text{Coriolis force}}{\text{Viscous force}} = \frac{2\rho\omega u}{\rho\nu\, \partial^2 u/\partial y^2} \sim \frac{\omega \bar{U}}{\nu\, \bar{U}/D^2} \sim \frac{\omega D^2}{\nu} \sim \frac{\omega D}{\bar{U}} \cdot \frac{\bar{U}D}{\nu} \sim \frac{\omega D}{\bar{U}}$$

Low flow rates and large spin rates would thus appear necessary for large rotational effects.

II. EXPERIMENTAL PROGRAM

The experimental investigations performed during this study were designed to measure differences in centerline velocity profiles and wall shear stresses, as well as overall pressure drop due to the rotation of rectangular channels. In addition, some off-centerline velocity profiles were measured, and an investigation of the distribution of u' turbulence was carried out on the centerline for each aspect ratio. The four aspect ratios tested were 1/2:1, 1:1, 4:1 and 7 1/3:1.

A. Apparatus

The apparatus was essentially the same as that used by Moon[12], but a modified test-section was used and improvements were made to the air-supply and rotational power systems. A general view is shown in Figure 1a, and a schematic of the test-section in Figure 2.

The spacing between the vertical Plexiglas test-plates was primarily chosen to allow fully-developed flow to be established, but had to be large enough for the flow to be investigated in some detail and to render negligible any variations in plate spacing along the test-section. A spacing of D = 3/4 inch was used for aspect ratios (Height, L/Width, D) 1:1, 4:1 and 7 1/3:1; while D = 1 1/2 inches was chosen for the 1/2:1 section. The top and bottom walls of the test-section were extruded aluminum channel sections bolted between the test-plates at the desired spacing and to an accuracy of $\pm$ .002 inches for the smallest sections and $\pm$ .007 inches for the largest.

The 72 inch long test-section was centrally mounted on a rotating horizontal aluminum plate and enclosed by a cylindrical Plexiglas cover to reduce the effect of rotation upon swirling of the room air. The

balanced test-rig was driven through V-belts by a 3 Hp D.C. Shunt Motor. An armature-resistance control and the variable excitation of a 250V D.C. generator were used to give a complete speed range from 30 - 210 rpm. The speed was measured using the linear voltage output of a General Electric Tachometer Generator driven by a flexible coupling in frictional contact with the main shaft (see Fig. 1c).

The air supply was provided by an axial-flow blower, rated at 250 cfm at 1 inch of water static (giving a maximum bulk velocity $\cong$ 60 ft/sec). The blower was hung from the laboratory ceiling vertically above the axis of rotation. A sheet-metal cone, with holes and spacers for bleeding-off excess air, delivered the flow to a 6 inch square sheet metal duct which led to a contraction immediately upstream of the test-section. Strips of tape placed on the walls to provide a smooth transition from the contraction and its variable fairing to the test-section also promoted turbulence. Honeycomb screens and flow aligners were placed in the guiding duct and at the inlet to the contraction to give a uniform velocity profile entering the test-section for all rotational speeds. In particular, a circular piece of honeycomb rotated in the exit of the sheet metal cone providing a steady air flow (see Appendix A1).

The measuring stations were located at x = 6, 42, 54 and 66 inches from the test-section inlet, midway between the top and bottom walls (hereafter called "the" centerline), and 1 inch above and below the centerline for the 4:1 and 7 1/3:1 sections.

B. Instrumentation

B.1 Pressure Measurements

The measuring probes are shown in Figure 1b. Mean velocity profiles

were measured with two total head probes constructed from hypodermic tubing and flattened to an outside height of .018 inches. Since transverses were only made from the suction side of the duct, one probe was bent slightly to allow investigation of the pressure side wall while the other was bent towards the suction side.

Transverse pressure gradients and probe blockage effects were measured with a static pressure probe of diameter .058 inches, the same as the main supporting tube for the total head probes. Also the wall static pressures were read on both sides of the duct centerline through tappings .020 inches diameter located axially every 6 inches.

The mechanism for traversing the probes consisted of a Selsyn generator and motor and reduction gears on the probe support (shown in Fig.1b). A small revolution-counter geared to the Selsyn generator gave an accurate reading of the probe position, and one revolution was equivalent to .006 inch.

Wall shear stresses were measured using two identical Preston tubes of .028 inches outside diameter, and six sublayer fences of the kind described by Goldberg[20]. A central step .006 inches high and .01 inches wide was machined on the end of a 3/16 inch diameter brass plug. Two static pressure tappings .020 inches diameter were situated on either side of the step which was normal to the flow when the fences were pressed into the walls of the test-section. The fences were situated on the centerline at axial distances x = 39, 51 and 63 inches.

A Pitot-static tube was located at the test-section inlet (x = 6 inches) and gave a measure of the bulk flow rate in the duct (see Appendix A2).

All pressure readings were transmitted from the rotating test-section by a rotary device developed in the Gas Turbine Laboratory and described in reference (11). Longer service was obtained using Army and Navy Specification "O" rings. Pressure differences were measured using the amplified signal from a Statham Δp pressure transducer of maximum range ± .05 psi. This transducer was calibrated (see Appendix A3) against an inclined manometer, and the axial pressure distributions were checked using a Meriam multi-tube manometer board inclined at an angle of 6.5°. The Preston tube reference static pressure tappings were located 1/4 inch from the duct centerline and these were also used as velocity head reference pressures as they were unaffected by the position of the probes.

B.2 Hot-wire Measurements

The constant temperature hot-wire system and apparatus were those used by Goldberg[20]. The amplifier and linearizer were powered by two 6 volt wet-cell batteries. The D.C. component of the linearizer output was monitored on a Heathkit VTVM and the fluctuating component on an RMS meter. The linearizer output was also displayed on an Oscilloscope and recorded on the x-axis of an X-Y Plotter, the y-axis of which was driven by a signal proportional to the distance between the duct walls.

Tungsten wire of .00015 inches diameter was used as the hot-wire. The ends of the wire were copper plated, leaving a bare section approximately .05 inches long and with a resistance of between 8 and 12 ohms. The wire was then soft-soldered perpendicular to the two supporting needles and close to the points. After linearizing the hot-wire response, the output signal corresponding to the duct maximum velocity at no-rotation was adjusted to a convenient value (1.5V). Signal readings

of u' turbulence on the RMS voltmeter, also recorded on the X-Y Plotter, could then be read directly as $\sqrt{u'^2}/U$.

C. Experimental Procedure

At each aspect ratio tests were performed with two Reynolds numbers of bulk mean velocities approximately 33 and 60 ft/sec. $\left(\frac{\rho \bar{U} d_h}{\mu} \cong 2 \times 10^4\right)$ Stationary and rotating checks were made on the inlet velocity profiles to ensure the bulk flow rate Q was maintained constant. Also, fully-developed flow was checked as closely as possible before recording velocity pressures, axial and transverse static pressure distributions and shear stress pressure differences, at various spin rates. The rotating electrical signal transmitter was checked for noise level and centerline u' measurements recorded.

C.1 Check on Fully-developed Flow

Claims of fully-developed flow can generally only be substantiated by measurements after the addition of an extra order of magnitude to the length of the duct or channel. Such procedure was impossible in this case and suffice had to be made of profile measurements at axial stations x = 42, 54 and 66 inches. In both the stationary and rotating checks made at all aspect ratios any differences observed were well within experimental accuracy (see Section IIE). Also there was close similarity between the stationary profiles on the suction and pressure sides. It was concluded that the flow was fully-developed at x = 54 inches, the measuring station where the majority of traverses and measurements were made.

C.2 Wall Shear Stresses

Four Preston tubes of diameters .072, .0575, .042 and .028 inches were tested to determine the effect of size in the constant shear-stress wall region. The correlation of Patel[21] was used to obtain shear stresses from the Preston tube Δp; no large differences were observed and the smallest tube was chosen as the least likely to be affected by departures from the Law of the Wall.

Each sublayer fence was calibrated (see Fig.3) using the .028 inch diameter Preston tube at various flow rates and no rotation. Although the fence measurements showed subsequent agreement in rotational tests the Preston tube was found to be a more sensitive indication of the wall shear stress as the pressure difference thus measured was approximately three times that measured by the fences.

D. Data Reduction

The velocity head data obtained from each transverse was in the form of amplified transducer signals of the difference between the total head pressure and the suction side wall static pressure. These readings were corrected with the transverse static pressure distribution (approximated as a linear variation between the measured wall static pressures) by a computer program which then gave values of:

$$\frac{u}{U}, \frac{u}{U_R}, \frac{v_x}{U}, \frac{\rho_{yU}}{\mu}, \frac{u}{u_\tau}, \frac{\rho y u_\tau}{\mu}$$

No other corrections were made to the velocity head readings and the friction velocity was calculated from the shear stress obtained using the Preston tube data. The sublayer fence readings were first converted to

equivalent Preston tube readings using Figure 3. The u' turbulence distribution ($\sqrt{u'^2}/U$) was found from a recording of the RMS value obtained using the X-Y Plotter. A mean line was passed through this trace and a correction made for the slipring noise level (see Fig.4) in the rotating cases.

E. Accuracy

Differences between rotational and no-rotational measurements were generally more accurately determined than the absolute magnitude of the measured quantities. The transducer gave velocity heads and static pressure differences with an accuracy better than 4% while the relative accuracy was estimated to be within 2% and the manometer board check within 1%. Velocity head measurements closer to the walls than about 2 probe heights (0.018 inches) were probably less accurate due to the wall effect. Preston tube Δp values were obtained with accuracy similar to the velocity head except for the lowest shear stresses where readings were small. Sublayer fence readings were always smaller than those of the Preston tubes so that their readings were probably less accurate.

The problem of drift and linearity in the hot-wire equipment were minimized by rapid transverses (3/4 inch per minute) and frequent calibration. The most significant error in the u' measurements was due to slipring noise which for the particular rings used was found to increase with speed. The maximum errors were thus of the order of 5% for no-rotation and 10% for maximum rotation. The rotational speed was maintained within 2% of the required value by use of the tachometer.

III. PRESENTATION AND DISCUSSION OF RESULTS

A. Velocity Profiles

The centerline (plane of mid-height) velocity profiles obtained with no rotation for the 1;1, 4;1 and 7 1/3:1 aspect ratios were found to agree within 2% when non-dimensionalized with the peak velocity. The profile is shown in Figure 5 and is plotted logarithmically in Figure 6 to give a comparison with the Law of the Wall. The Law of the Wall region is fitted well by the correlation

$$\frac{u}{u_\tau} = A \log \frac{\rho y u_\tau}{\mu} + B$$

where A = 5.6 and B = 4.9 as suggested by Clauser[22], and u_τ is calculated from the Preston tube wall shear stress. The measurements were obtained from the edge of the laminar sublayer, but show a wake region quite clearly.

The 1/2:1 profile **obtained** with no rotation is shown in Figures 7 and 8 and exhibits a region of uniform axial velocity as well as the Law of the Wall and wake regions. (The 1/2:1 profiles were plotted separately because of the difference in no-rotational velocity profiles).

Figures 5 to 8 also show the general effects of rotation on the centerline velocity distribution for the four aspect ratios. Large effects on both velocity profile and wall shear stress are noticed for the 1:1 duct and especially for the 1/2:1 duct. The velocity on the pressure side is markedly increased by rotation at these aspect ratios and the shear stress is correspondingly higher. On the suction side the effect of rotation is to decrease the velocity and the wall shear stress. Also the peak velocity moves toward the pressure side and there appears

a slight deficiency in the integrated centerline flow. These results may be qualitatively explained by the mechanism of secondary flow which transfers low momentum fluid from the low velocity regions near the top and bottom walls to the suction side of the duct. The deficiency in the integrated centerline flow will be reconsidered in Sections IIIC and IIIF.5.

The effects of rotation on the 4:1 and 7 1/3:1 profiles are much less pronounced, and are almost within experimental error for the 7 1/3:1 aspect ratio. The peak velocity appears slightly displaced to the suction side and the integrated centerline flow is somewhat lower than for no rotation. Indeed the profiles are quite similar to the fully-developed curved duct profiles of Eskinazi and Yeh[4].

Comparison with the Law of the Wall, shown in Figures 6 and 8, shows that the pressure side retains a logarithmic region for all aspect ratios while the suction side exhibits this universality only for the 4:1 and 7 1/3:1 ducts. The suction sides of the 1:1 and 1/2:1 ducts depart from the Law of the Wall in a manner similar to boundary layers in adverse pressure gradients, the effect being largest for the greatest spin parameters $\omega D/\bar{U}$, when very little logarithmic profile remained. The experimental accuracy on the suction side is however lower than on the pressure side because the velocity head is much smaller, and this undoubtedly affected both the Preston and Pitot tube readings. Indeed for the low R_{e_L} measurements the velocity heads were low at all points.

B. Secondary Axial Velocities

A measure of the effect of rotation on the flow can be obtained by subtracting the no-rotation velocity profile from the rotational profile to give the secondary axial velocity. Also the relative accuracy of the

velocity measurements was probably better than their absolute accuracy which suggests the use of this method of comparison.

The secondary axial velocities, non-dimensionalized with the no-rotation peak velocity, are shown in Figures 9 and 10 for two values of Reynolds number (equivalent to $\overline{U}$ = 33 ft/sec and 60 ft/sec approximately) and various spin rates at each aspect ratio. Generally the velocity differences increase in a roughly linear manner for low spin rates, the changes becoming much smaller at high spin rates. The rotational changes in velocity profile previously shown in Figure 5 are now plotted in Figure 11 and it can be seen that the effect of increasing the aspect ratio is to decrease the secondary axial velocities. A better picture of the effect of aspect ratio on the centerline secondary axial velocities is obtained by defining a momentum parameter

$$\xi = \frac{1}{D} \int_{-D/2}^{D/2} \left(\frac{u_x}{U} \right)^2 dy$$

The values of this parameter for the two series of tests at each aspect ratio are plotted in Figure 12, and re-plotted against aspect ratio in Figure 13. Again the largest and only really significant effects are seen to occur at the small aspect ratios. These findings would seem to support the idea that secondary flows are the dominant factor in rotational duct-flows with the present range of spin parameters.

C. Off-centerline Velocities

A feature of the centerline secondary velocities is that more momentum is lost on the suction side than is gained on the pressure side. This centerline loss of momentum was checked at the 4:1 and 7 1/3:1 aspect ratios

where a **traversing** station 1 inch from the centerline was available.

The results are shown plotted in Figure 14 and it can be seen that there is now a surfeit of momentum on the pressure side. Thus it appears that the observations for the whole duct can be explained without violation of continuity by a transfer of low momentum fluid to the centerline of the duct. This would also seem to support the postulated mechanism of secondary circulations.

D. Calculation of Turbulent Flows

The equations of motion for the turbulent flow of a fluid are generally much more complex than the corresponding equations for laminar flow with uniform viscosity. They include the so-called Reynolds' stresses. Sometimes, however, the only significant contribution of the turbulence is to increase the shear stress, albeit in a non-uniform manner. In a strictly two-dimensional flow only one shear stress appears and it has been found possible to represent the mean characteristics of the flow by a region of uniform eddy viscosity ν (where $-\overline{u'v'} = \nu \frac{\partial u}{\partial y}$) extending over the majority of the boundary layer thickness, and a slip velocity region at the wall. The uniform eddy viscosity in the outer portion of a turbulent boundary layer arises as a result of the shearing stress being carried by the large eddies of the turbulent flow, and the fact that the characteristic size of these eddies in this region is a nearly fixed fraction of the boundary layer thickness.

Application of a similar procedure to a rectangular duct flow involves the further assumption of an isotropic eddy viscosity unless the component equations are treated separately. Furthermore, it is known that for turbulent flow in rectangular channels the Reynolds' stresses

give rise to secondary effects even without rotation, bending, etc:. These effects are largest in the corners and distort the axial velocity distribution in such regions. The present analysis is primarily concerned with a calculation of the centerline velocity distribution together with a qualitative representation of the complete flow. It was hoped that, with only these limited objectives in mind, a slip velocity model of the flow of a fluid with uniform, isotropic eddy viscosity would yield some useful results and a better understanding of the problem.

E. Calculation of Flow in Rotating Channels

The analysis of fully-developed laminar flow in straight channels placed in a rotating reference frame has been studied by Barua[16] and Benton[14] who concerned themselves with a circular pipe, and more recently by Boyer[17] who considered a rectangular channel. In each case the channel rotates at constant angular velocity about an axis perpendicular to the channel axis, as illustrated in the sketch opposite.

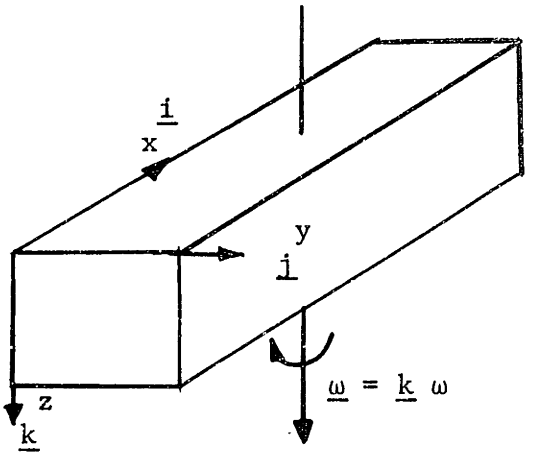

The equations of motion for the steady flow of an incompressible fluid with uniform viscosity in this case may be written in the form

$$(\underline{V} \cdot \nabla)\,\underline{V} = -2\,\underline{\omega} \times \underline{V} - \nabla\Phi + \nu\nabla^2\underline{V} \qquad (1)$$

where $\Phi = \frac{p}{\rho} - \frac{\omega^2 r^2}{2}$, r is the distance from the axis of rotation and gravity is neglected.

Benton, who was interested in the effects of the earth's rotation on pipe flow, immediately linearized the equations by assuming the components

and derivatives of the perturbation velocity to be small compared with the conventional solution for laminar flow in a straight pipe. He then proceeded to compute the secondary velocity components, in particular the component in the axial direction. The stream function associated with velocities in the y-z plane was found to be proportional to the ratio of the Reynolds number to the Rossby Number*, i.e. $R = \frac{R_e}{R_o} = \frac{UD\rho}{\mu}$. $\frac{2\omega D}{U} = \frac{2\omega D^2\rho}{\mu}$, which is itself proportional to the ratio of the Coriolis and frictional forces. As Coriolis forces increase in relative magnitude the secondary flow appears and strengthens.

The perturbation of the axial velocity non-dimensionalized with the no-rotational peak velocity was found to be proportional to $K = \frac{R_e^2}{R_o} = \frac{2\omega D^3 U\rho^2}{\mu^2}$. This secondary axial velocity was found to be significant for $K > 5 \times 10^2$ while the linearization only appeared applicable for $K < 10^3$.

Barua used a modification of a theory used by Dean[15] to calculate the effect of curvature on fully-developed laminar flow in a curved pipe. The method involves expanding the axial velocity and the stream function as power series in a dimensionless constant found from the non-dimensional equations of motion. The constant used by Barua was $R = \frac{2\omega D^2\rho}{\mu}$ and he carried his calculations as far as the Second Order terms in R. It shculd be noted that the First Order equations and their solutions are the same as those obtained by Benton, and thus the range of rotational speeds for which the solution is applicable will be the same, or alternatively the power series is convergent. If the First Order solution was not a close estimate of the true perturbation velocity the Second Order

*Rossby Number - a non-dimensional ratio, $\frac{v}{2\omega D}$, found useful in meteorology and oceanography

would necessarily be large and the power series would not converge.

Both of the theories just considered apply for small spin rates. At the other extreme Boyer studied the problem of the effect of large rotation rates on laminar flow in a rectangular channel. He found that for $R = \frac{2\omega L^2 \rho}{\mu} >> 1$ and $R_e (= \frac{\rho UL}{\mu}) << R^{1/2}$ the channel flow is of a boundary layer type in which the regions of large shear are restricted to the neighborhood of the channel walls. Values of $R \cong 2 \times 10^4$ and thus $R_e = 1.0$ were suggested as necessary for this type of flow.

Table 1 - Approximate Experimental Spin Parameter Ranges Based on Uniform, Isotropic Estimate of Turbulent Eddy Viscosity

Aspect Ratio L/D	Range of $\frac{2\omega D^3 U}{\nu^2}$	Range of $\frac{2\omega L^3 U}{\nu^2}$	$R = \frac{2\omega L^2}{\nu}$	$\frac{UL}{\nu}$
1/2:1	$0 \rightarrow 2 \times 10^5$	$0 \rightarrow 2 \times 10^4$	$0 \rightarrow 30$	750
1:1	$0 \rightarrow 2 \times 10^4$	$0 \rightarrow 2 \times 10^4$	$0 \rightarrow 30$	750
4:1	$0 \rightarrow 2 \times 10^4$	$0 \rightarrow 1.3 \times 10^6$	$0 \rightarrow 400$	3000
7 1/3:1	$0 \rightarrow 2 \times 10^4$	$0 \rightarrow 8 \times 10^6$	$0 \rightarrow 2000$	5000

Table 1 reviews the ranges of the above-mentioned spin parameters which were obtained during the present series of tests. The major factor in producing such large ranges, was the variation in the rotational speed ω. The procedure proposed for estimating the eddy viscosity is described in Section IIIF.2, but for these estimates a value of $\nu = .005$ ft/sec was selected. It is seen that the Reynolds number $(\frac{UL}{\nu})$ is very much larger than that required for the flow regime considered by Boyer while the values of R are too small except possibly for the highest spin rates at L/D = 7 1/3:1.

The experimental range of $\frac{2\omega L^3 U}{\nu^2}$ is now compared with the range of applicability found by Benton for his First Order theory. As the parameter $\frac{R_e}{R_o}$ increased from 10^3 to 5×10^3 Benton found that the assumptions made during linearization became less tenable, thus one would expect the Second Order terms of Barua's theory to increase in relative magnitude until they eventually dominate (the series becomes divergent). The calculation of the present turbulent flow involved the use of a slip velocity at the wall, and an approximation of the actual velocity profile with no rotation. It was tentatively hoped that these modifications, when included in a calculation as far as the Second Order terms, would give results applying, at least for the 1/2:1 and 1:1 ducts, over a significant range of the measurements. It was also hoped that such calculations would lead to a better understanding of the problem.

F. Calculation of Secondary Axial Velocities

The equations of motion were written in Section IIIE and are here repeated for convenience.

$$\underline{V} \cdot \nabla \underline{V} = -2\, \underline{\omega} \times \underline{V} - \nabla\Phi + \nu\nabla^2\underline{V} \tag{1}$$

Also the equation of continuity may be written as

$$\nabla \cdot \underline{V} = 0 \tag{2}$$

If the assumption of fully-developed flow is now introduced, the velocity may be written in terms of a stream function ψ associated with the velocity components in the plane normal to the axis of the channel,

$$\underline{V} = \underline{i}\, u - \nabla \times \underline{\psi} \qquad \text{where } \underline{\psi} = \underline{i}\psi \tag{3}$$

or

$$\underline{V} = \underline{i}\, u - \underline{j}\, \frac{\partial \psi}{\partial z} + \underline{k}\, \frac{\partial \psi}{\partial y} \tag{4}$$

The vector directions $\underline{i}$, $\underline{j}$, $\underline{k}$ are defined in Section IIIE and substitution of equation (4) into equation (1) yields the three component equations of motion as

$$-\frac{\partial\psi}{\partial z}\frac{\partial u}{\partial y}+\frac{\partial\psi}{\partial y}\frac{\partial u}{\partial z}=-2\omega\frac{\partial\psi}{\partial z}+\nu\nabla^2 u-\frac{\partial\Phi}{\partial x} \tag{5}$$

$$\frac{\partial\psi}{\partial z}\frac{\partial^2\psi}{\partial z\partial y}-\frac{\partial\psi}{\partial y}\frac{\partial^2\psi}{\partial z^2}=-2\,\omega u-\nu\nabla^2\left(\frac{\partial\psi}{\partial z}\right)-\frac{\partial\Phi}{\partial y} \tag{6}$$

$$-\frac{\partial\psi}{\partial z}\frac{\partial^2\psi}{\partial y^2}+\frac{\partial\psi}{\partial y}\frac{\partial^2\psi}{\partial y\partial z}=+\nu\nabla^2\left(\frac{\partial\psi}{\partial y}\right)-\frac{\partial\Phi}{\partial z} \tag{7}$$

The potential term may be eliminated from equation (6) and (7) to give

$$\left(\frac{\partial\psi}{\partial z}\frac{\partial}{\partial y}-\frac{\partial\psi}{\partial y}\frac{\partial}{\partial z}\right)\nabla^2\psi=-2\omega\frac{\partial u}{\partial z}-\nu\nabla^4\psi \tag{8}$$

Equations (5) and (8) may be put in a non-dimensional form in a manner similar to that given by Dean, using

$$\psi'=\frac{\psi}{\nu}\,,\quad u'=\frac{u}{U}\,,\quad x'=\frac{x}{D}\,,\quad y'=\frac{y}{D}\,,\quad z'=\frac{z}{L}$$

where L and D are the rectangular duct height and width, respectively, and U is the peak axial velocity for no-rotation. Equations (5) and (8) become

$$\left(\frac{D}{L}\right)\left[\frac{\partial\psi}{\partial z}\frac{\partial}{\partial y}-\frac{\partial\psi}{\partial y}\frac{\partial}{\partial z}\right]\nabla^2\psi=-K\left(\frac{D}{L}\right)\frac{\partial u}{\partial z}-\nabla^4\psi \tag{9}$$

$$\left(\frac{D}{L}\right)\left[-\frac{\partial\psi}{\partial z}\frac{\partial u}{\partial y}+\frac{\partial\psi}{\partial y}\frac{\partial u}{\partial z}\right]=-2\frac{\omega D}{U}\left(\frac{D}{L}\right)\frac{\partial\psi}{\partial z}+\nabla^2 u-C \tag{10}$$

where $K=\frac{2\omega D^3 U}{\nu^2}$, $C=\frac{\partial\Phi}{\partial x}\cdot\frac{D}{\nu U}$, and $\nabla^2=\left(\frac{\partial^2}{\partial y^2}+\frac{D^2}{L^2}\frac{\partial^2}{\partial z^2}\right)$

It should be noted that, after non-dimensionalizing, the primes are omitted.

It is now assumed that the solution to these equations can be written in the (dimensionless) form:

$$\begin{aligned} u &= u_o + Ku_1 + K^2u_2 + \ldots \\ \psi &= \quad K\psi_1 + K^2\psi_2 + \ldots \\ C &= C_o + KC_1 + K^2C_2 + \ldots \end{aligned} \tag{11}$$

The relations (11) are substituted into equations (9) and (10) and the coefficients of equal powers of K are equated to give

$$\nu \nabla^2 u_o = \frac{\partial \Phi_o}{\partial x} \tag{12}$$

$$\nu \nabla^2 u_1 = \frac{\partial \Phi_1}{\partial x} - \frac{\partial \psi_1}{\partial z}\frac{\partial u_o}{\partial y} + \frac{\partial \psi_1}{\partial y}\frac{\partial u_o}{\partial z} \tag{13}$$

$$\nu \nabla^2 u_2 = \frac{\partial \Phi_2}{\partial x} - \frac{\partial \psi_1}{\partial z}\frac{\partial u_1}{\partial y} - \frac{\partial \psi_2}{\partial z}\frac{\partial u_o}{\partial y} + \frac{\partial \psi_1}{\partial y}\frac{\partial u_1}{\partial z} + \frac{\partial \psi_2}{\partial y}\frac{\partial u_o}{\partial z} + 2\omega \frac{\partial \psi_1}{\partial z} \tag{14}$$

$$\nu \nabla^4 \psi_1 = -2\omega \frac{\partial u_o}{\partial z} \tag{15}$$

$$\nu \nabla^4 \psi_2 = -\left[\frac{\partial \psi_1}{\partial z}\frac{\partial}{\partial y} - \frac{\partial \psi_1}{\partial y}\frac{\partial}{\partial z}\right] \nabla^2 \psi_1 - 2\omega \frac{\partial u_1}{\partial z} \tag{16}$$

These equations are written in a dimensional form to show the dependence on ω and ν more clearly. It may be noted here that equivalent dimensionless equations and thus the same solutions are obtained for other non-dimensionalizing procedures.

The method of solution adopted was to choose a no-rotational velocity profile u_o and a value for the eddy viscosity corresponding to a given primary flow and then successively calculate ψ_1, u_1, ψ_2 and u_2. Separate calculations were necessary for each aspect ratio and each set of boundary conditions.

F.1 Axial Velocity Distribution $u_o(y,z)$

Leutheusser[23] conducted an experimental study of the centerline flows of rectangular ducts of 1:1 and 3:1 aspect ratios for the Reynolds Number range between 10^4 and 10^5. He concluded there is "strong evidence in favor of the same universal inner law of velocity distribution which applies also to other turbulent shear flows", however "the range of the agreement over which the velocity distribution is distinctly logarithmic is limited in extent in the case of rectangular conduits". The limitation on the extent of inner law correlation appears in doubt and no existence of an outer law profile was found.

The Reynolds' stresses are the main factor causing the profiles to be non-universal since they interact to cause secondary flows which are largest near the corners. Here however the Reynolds' stresses are omitted from the equations of motion and the velocity distribution $u_o(y, z)$ must therefore be a close approximation to that measured for stationary channels. It was noted from measurements of velocity profiles on the longer centerline of a rectangular channel that a region of uniform velocity existed. The symmetrical velocity profile for the whole duct (see sketch opposite) was thus represented as

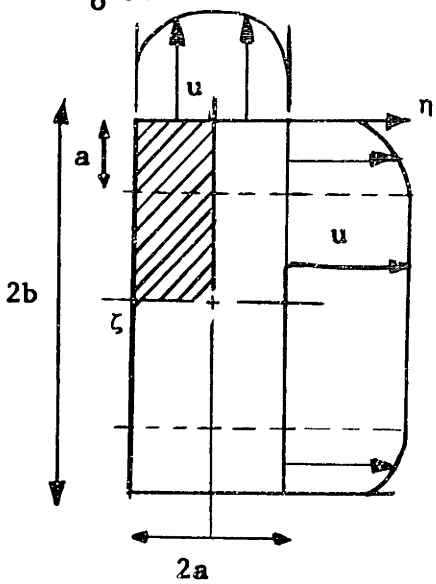

$$u_o(\eta, \zeta) = f_1(\frac{\eta}{a}) \quad f_2(\frac{\zeta}{b}) \tag{17}$$

where η is the coordinate of the shorter dimension and the function f_1 corresponds to the measured centerline profile for no rotation, shown

graphically in Figure 7. For the shaded quadrant, for example

$$f_2(\frac{\zeta}{b}) = f_1(\frac{\zeta}{a}) \qquad 0 < z < a$$

$$1 \qquad a < z < b$$

A wall slip velocity was assumed for the function f_1 and taken to be

$$f_1\ (\frac{y}{a} = 0) = 0.40$$

F.2. Estimation of Eddy Viscosity

It has already been seen that the term dominating the secondary axial velocity is proportional to $K \sim \nu^{-2}$. Thus there is a strong dependence on the eddy viscosity and indeed its determination is the major limitation of this analysis. A simplifying assumption of uniform isotropic eddy viscosity has been tacitly introduced in the analysis so far presented and was briefly discussed in Section IIID. This discussion will be continued in Appendix B.1, where possible alternative methods are suggested.

Moses[18] provides a very approximate equation for the eddy viscosity at $y = \delta/2$ is a two-dimensional turbulent boundary layer of thickness, δ,

$$\frac{\nu}{U\delta} = \frac{.004}{\text{Log } R_{e_\delta} - 7.6} + 0.0013 \qquad (18)$$

The use of this equation for estimating the eddy viscosity requires the selection of an equivalent boundary layer thickness which can be used for rectangular ducts of aspect ratios between 1/2:1 and 7 1/3:1. Consistent with our assumptions concerning the velocity profile in rectangular channels we may consider the "boundary layer" thickness to be

half of the smallest dimension of the duct. This was the procedure finally adopted.

F.3 Boundary Conditions - Wall Slip Velocity

If it is assumed that the flow near the wall can be represented as a thin laminar sublayer adjoining the main flow field, which in the present analysis has uniform eddy viscosity, and if it is further assumed that a region of constant shear stress extends from the wall to contain this junction, the shear stress at the junction may be written as

$$\tau_o = \mu \frac{u_{slip}}{\Delta_{sub}} = \rho\nu\left(\frac{\partial u}{\partial y}\right)_{y=0} \tag{19}$$

At the duct centerline the wall shear stress was measured experimentally and from the velocity profile an arbitrary $u_{slip} = 0.40\ U$ was chosen to give the sublayer thickness

$$\Delta_{sub} = \frac{\mu\, u_{slip}}{\tau_o} \tag{20}$$

Now with the assumption that the sublayer has uniform thickness independent of rotation a boundary condition is obtained such that

$$u_{slip} = (u)_{y=0} = B_k \left(\frac{\partial u}{\partial y}\right)_{y=0} \tag{21}$$

where

$$B_k = \frac{\rho\, \nu\, \Delta_{sub}}{\mu} \tag{22}$$

The eddy viscosity has already been assumed to be determined by the primary flow, u_o, and to be independent of rotation so, if we notice that the sublayer thickness and laminar viscosity are the same for the secondary circulations, this relation provides a boundary condition for the stream function ψ also.

The boundary conditions for equations (12)-(16) found using this slip-velocity model and the condition of no flow normal to the wall are (in dimensionless form)

$$\underset{D}{y} = \underset{(1)}{0} \;,\; u = \underset{(-)}{+} B_k \frac{\partial u}{\partial y} \;,\; \frac{\partial \psi}{\partial y} = \underset{(-)}{+} B_k \frac{\partial^2 \psi}{\partial y^2} \;,\; \frac{\partial \psi}{\partial z} = 0$$

$$\underset{L}{z} = \underset{(1)}{0} \;,\; u = \underset{(-)}{+} B_k \frac{\partial u}{\partial z} \;,\; \frac{\partial \psi}{\partial z} = \underset{(-)}{+} B_k \frac{\partial^2 \psi}{\partial z^2} \;,\; \frac{\partial \psi}{\partial y} = 0$$

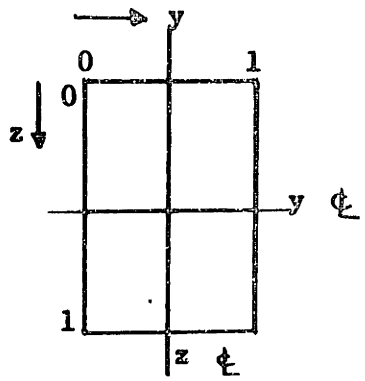

Also we can arbitrarily specify $\psi = 0$ at the walls.

F.4 Symmetry Conditions

The symmetry relations for the velocity and stream function contributions u_1, u_2 and ψ_1, ψ_2 may be obtained from a consideration of equations (13)-(16) knowing that u_o is symmetrical about both centerlines of the rectangular duct and that the boundary conditions are symmetrical also.

Term	Even Function in y	Even Function in z
u_1	X	✓
u_2	✓	✓
ψ_1	✓	X
ψ_2	X	X

Table 2

Thus it is found already that

$$\int_A u_1 \, dA = 0 \quad \text{and} \quad C_1 = 0 \tag{23}$$

and that for a constant bulk flow rate we must require

$$\int_A u_2 \, dA = 0 \tag{24}$$

F.5 Method of Solution and Results

A relaxation method of solution was applied to equations (13)-(16) written in difference form. The symmetry conditions of Section IIIF.4 were used so that only one quadrant of the rectangular cross-section need be treated, and the condition (24) was applied to ensure the bulk flow remained constant. The quadrant was split into a 10 x 10 mesh and values of u_1, u_2, ψ_1 and ψ_2 were obtained at each mesh point.

The desired secondary axial velocities are given by equation (11). The variation of the maximum positive and maximum negative secondary axial velocities with rotation may be used to obtain the range of applicability of the theory. The experimental variations and those predicted by the theory at the plane of mid-height for the $\frac{1}{2}$:1 aspect ratio are plotted in Figure 15a.

There is good agreement only at low values of the spin parameter, and this was obtained by changing the value of the eddy viscosity from that predicted in Section IIIF.2 to give a better agreement. Small changes could be made without changing the constant in the boundary

conditions since the results were relatively insensitive to that constant (see Figure 15d). The insensitivity also shows that the assumptions made in Section IIIF.3 while developing the slip-velocity model are not too critical. Further it was found that the final term in equation (14) produced only small changes in u_2 which allows the assumption that u_2 is proportional to $\frac{1}{\nu^4}$ as suggested by equation (11). Thus it is possible to obtain the results for different spin rates, ω, and different eddy viscosities, ν, from a single calculation at each aspect ratio. The actual change made to the eddy viscosity ν was from .007 ft^2/sec to .0039 for the 1/2:1 duct.

A comparison of the complete secondary axial velocity distribution at the plane of mid-height is given in Figures 15b and 15c for the 1/2:1 and 1:1 aspect ratios. The 1/2:1 calculations correspond to $\frac{\omega D}{U} = .0076$ in Figure 15a, and the values calculated for 1:1 correspond to an eddy viscosity of .0035 compared with .0065 predicted in Section IIIF.2. The terms contributing to the secondary axial velocity are plotted separately and also when added together. Ku_1 is seen to be symmetrical about the center of the duct while K^2u_2 contributes the decrease in centerline axial momentum observed throughout the measurements.

The agreement obtained between the shapes of the measured and calculated profiles is remarkably good and lends some justification to the assumptions made about the eddy viscosity and the velocity distribution.

The dimensionless stream function ψ is shown in Figure 16 and it can be seen that the Second Order term $K^2\psi_2$ contributes a very small change in the First Order term $K\psi_1$. The regions where the velocities in the

y-z plane are maximum are seen to be the top and bottom walls but the velocities close to the centerline are only slightly smaller.

G. Wall Shear Stresses

The variation in shear stress caused by rotation is probably the most significant of the relative effects of Coriolis instability and Secondary Flow. At the plane of mid-height, the effect of Coriolis on the stability of the flow and thus on the momentum transport and shear stresses should be unaffected by changes in aspect ratio, as long as the flow in this plane is closely two-dimensional. Also the relative importance of secondary flows if present should be apparent from the measured changes in centerline skin-friction.

Both the Preston tube and the Clauser method[22] for determining shear stress from the measured velocity profile depend upon the Law of the Wall being valid. Table 3 shows that good agreement is obtained between the two methods for all aspect ratios on the pressure side, especially at the higher Reynolds number (R_{e_L}) where more accurate readings were possible. This agreement is probably the result of the pressure side retaining a logarithmic portion for all aspect ratios as seen in Figures 6 and 8. The most serious differences in shear stress coefficient occur with large spin rates on the suction surfaces of the 1/2:1 and 1:1 aspect ratios, where the logarithmic region is seriously in question, and where the measurement of the Preston tube Δp is relatively less accurate.

Figure 17 shows the non-dimensional skin-friction coefficients obtained by the Preston tube for the four aspect ratios tested. Large changes in shear stress are observed only for the 1:1 and 1/2:1 ducts

suggesting the importance of secondary flows; the 7 1/3: 1 duct shows a maximum change of only 15%. The variation in shear stress for the 4:1 duct is intermediate between the weakly influenced large aspect ratios and the strongly influenced small aspect ratios. Figure 18 indicates that the influence of the end walls has not reached an asymptotic limit at the 7 1/3:1 aspect ratio.

In the range of $\omega D/\overline{U}$ measured the rotational effect is roughly proportional to the spin parameter and equal changes are noticed on the pressure and suction sides. These observations are also shown in Figure 19 where the mean centerline skin-friction coefficient is seen to be sensibly constant for all aspect ratios and values of the spin parameter, and the ratio of the pressure to suction side shear stresses varies approximately linearly with $\omega D/\overline{U}$ for each aspect ratio.

H. Turbulence Intensities

The measured variation of u' turbulence intensity with rotation are plotted in Figure 20 for the 1/2:1, 1:1 and 7 1/3:1 aspect ratio ducts. Quite large changes are observed at 1/2:1 and 1:1 and the distribution for no-rotation may be considered to be affected in two distinct ways. The turbulence intensity on the pressure side decreases with rotation, while a convective transport conveys turbulent energy from the suction side to the center portion of the duct. Comparatively small changes, almost within experimental error, occur at the 7 1/3 :1 aspect ratio.

Let us consider the flow in the plane of mid-height of the duct, and allow the flow to have mean and turbulent velocity and pressure components, i.e. $u = \overline{u} + u'$; $v = \overline{v} + v'$; $w = \overline{w} + w'$; $p = \overline{p} + p'$. Symmetry in the z-direction and the assumption of fully-developed flow

make $\bar{w}$, and the z and x derivatives of mean quantities all zero. If triple correlations of turbulence intensities are ignored, the energies associated with the x, y and z components of turbulent fluctuations may be expressed by the equations

$$\frac{\bar{v}}{2}\frac{\partial(\overline{u'^2})}{\partial y} = -(\overline{u'v'})\left[\frac{\partial \bar{u}}{\partial y} - 2\omega\right] - \frac{1}{\rho}\overline{u'\frac{\partial p'}{\partial x}} + \frac{\mu}{\rho}\left[\overline{u'\frac{\partial^2 u'}{\partial y^2}} + \overline{u'\frac{\partial^2 u'}{\partial z^2}}\right]$$

$$\frac{\bar{v}}{2}\frac{\partial(\overline{v'^2})}{\partial y} + (\overline{v'^2})\frac{\partial \bar{v}}{\partial y} = -2\omega(\overline{u'v'}) - \frac{1}{\rho}\overline{v'\frac{\partial p'}{\partial y}} + \frac{\mu}{\rho}\left[\overline{v'\frac{\partial^2 v'}{\partial y^2}} + \overline{v'\frac{\partial^2 v'}{\partial z^2}}\right]$$

$$\frac{\bar{v}}{2}\frac{\partial(\overline{w'^2})}{\partial y} = \frac{1}{\rho}\overline{w'\frac{\partial p'}{\partial z}} + \frac{\mu}{\rho}\left[\overline{w'\frac{\partial^2 w'}{\partial y^2}} + \overline{w'\frac{\partial^2 w'}{\partial z^2}}\right]$$

The first term on the right hand side of the equations represents the production of turbulence and is seen to be modified by rotation such that a transfer of energy occurs between the x and y components. On the pressure side of the duct $(-\overline{u'v'})$ is positive and thus u' turbulent energy tends to be dissipated. This effect was observed experimentally. The first term on the left hand side of the equations constitutes the transport of energy by mean motion, in this case directed from one side of the duct towards the other. Thus, combined with the earlier observations concerning secondary flows, which at the centerline are directed from the suction surface to the pressure surface, we have a possible explanation for the observed convection of u' energy from the suction surface towards the center of the channel.

IV. CONCLUSIONS

The centerline effects of rotation on the velocity profile, wall shear stresses, and u' velocity distributions were all strongly dependent on aspect ratio. At the 1/2:1 and 1:1 aspect ratios large effects occurred, while much smaller effects were observed at 4:1 and 7 1/3:1. These results suggest that, for spin rates up to $\omega D/\overline{U} = 0.08$, the most important effects of rotation are due to secondary flows, and not Coriolis instability. Also a loss of momentum in the integrated centerline velocity profile agrees with the postulated transfer of axial momentum due to secondary circulations. The impellers of centrifugal compressors operate near the present range of spin-parameter and, while the flow in these is not fully-developed, the results indicate that large modifications to the exit velocity profile are possible, and predict their nature qualitatively.

Calculations of fully-developed turbulent flow in rectangular channels, using an extension of a theory used to predict rotational changes in laminar pipe flow, have shown the usefulness of the assumption of a uniform, isotropic eddy viscosity. They showed a decrease in integrated centerline momentum and changes in axial pressure drop as Second Order effects. The analysis which only applies to low angular velocities was in good qualitative agreement with the measurements, and if the eddy viscosity was suitably chosen quantitative agreement could be obtained also.

The secondary axial velocities varied linearly with spin rate at low spin-parameters; at high spin rates the increments became smaller. The variation of centerline wall shear stress with spin-parameter was

approximately linear for the whole range and the mean centerline value remained closely constant, u' turbulence intensities changed only at the 1/2:1 and 1:1 aspect ratios, there being a decrease on the pressure side and an apparent convection towards the center of the duct from the suction side; the latter observation may be explained by secondary flows.

Friction factor changes due to rotation were small at all aspect ratios, being largest for the square channel. An extension, to rectangular ducts, of an analogy between flows in rotating, bent and heated horizontal pipes appears to be limited because secondary flows, the basis of the analogy, depend on aspect ratio. The square channel data was however in good agreement with data for rotating and bent circular pipes.

V. SUGGESTIONS FOR FURTHER WORK

The velocity profile and eddy viscosity are better known for a circular pipe than any other channel, and the present calculations and experimental procedure could be applied to fully-developed flow in a rotating pipe. The whole field of developing flows in different geometries including straight radial ducts awaits calculation, and experiment at practically important spin rates. Also confident use of the analogy between rotating, bent and heated horizontal channels requires an accurate experimental study of its limitations.

REFERENCES

1. Trefethen, L. MacG. - "Fluid Flow in Radial Rotating Tubes" Actes, IX^{e} Congres Internation de Mechanique Appliquee, Vol.II pp. 341-350 - Univ. de Bruxelles, 1957.

2. Trefethen, L. MacG. - "Flow in Rotating Radial Ducts: Report R55GL350 on Laminar Flow in Rotating, Heated Horizontal and Bent Tubes, Extended into Transition and Turbulent Regions" - General Electric Co. Report No. 55GL350-A, August 1957.

3. Liepmann, H.W. - "Investigations on Laminar Boundary Layer Stability and Transition on Curved Boundaries" - NACA Wartime Report W-107, August 1943.

4. Eskinaze, S. and Yeh, H. - "An Investigation on Fully-developed Turbulent Flows in Curved Channels" - J. of Aero Science, Vol. 23, No. 1, pp 23-34, January 1956.

5. Margiolis, D.P. and Lumley, J.L. - "Curved Turbulent Mixing Layer" The Physics of Fluids, Vol. 8, No. 10, October 1965.

6. Rayleigh, J.W.S. - "On the Dynamics of a Revolving Fluid" - Proc. Royal Soc., Vol. 6A, pp 148-154, 1916.

7. Prandtl, L. - "Effect of Stabilizing Forces on Turbulence:" NACA TM NO. 625, 1931.

8. Work in progress at Stanford University on Stability Effects of Coriolis in a Rotating Water Channel.

9. Thomson, J. - "On the Origins of Windings of Rivers,etc." Proc. Royal Soc., Vol.25, 1876.

10. Thomson, J. - "Experimental Demonstration in Respect to the Origin of Windings of Rivers, etc." Proc. Royal Soc., Vol. 26A, p. 356, 1877.

11. Hill, P.G. and Moon, I.M. - "Effects of Coriolis on the Turbulent Boundary Layer in Rotating Fluid Machines" - Gas Turbine Laboratory Report No. 69, MIT, June 1962.

12. Moon, I.M. - "Effect of Coriolis Force on the Turbulent Boundary Layer in Rotating Fluid Machines" - Gas Turbine Laboratory Report No. 74, MIT, June 1964.

13. Lohmann, R.P. - "An Investigation of the Influence of the Boundary Layers on the Performance of Centrifugal-Compressor Impellers" Trans. ASME - J. of Basic Engineering, Vol.88, Series D, No.1, March 1966.

14. Benton, G.S. - "The Effect of the Earth's Rotation on Laminar Flow in Pipes" - J. of Appl. Mechanics, Vol. 23, No.1, pp. 123-127, March 1956.

15. Dean, W.R. - "The Streamline Motion of Fluid in a Curved Pipe" Phil. Mag., Vol. 5, pp 673-695 - London, 1928.

16. Barua, S.N. - "Secondary Flow in a Rotating Straight Pipe" Proc. Royal Soc. A, Vol.227, pp 133-139, 1954.

17. Boyer, D.L. - "Flow Through a Rapidly Rotating Rectangular Channel" Ph.D. Thesis, the Johns Hopkins Univ., 1965.

18. Moses, H.L. - "The Behavior of Turbulent Boundary Layers in Adverse Pressure Gradients" - Gas Turbine Laboratory Report No. 73, MIT, January 1964.

19. Clauser, F.H. - "The Turbulent Boundary Layer" - Adv. in Appl. Mechanics, Vol. 4, 1956.

20. Goldberg, P. - "Upstream History and Apparent Stress in Turbulent Boundary Layers" - Gas Turbine Laboratory Report No. 85 MIT, May 1966.

21. Patel, V.C. - "Calibration of the Preston Tube and Limitations on its Use in Pressure Gradients" - J. Fl. Mech., Vol. 23, Part 1, 1965.

22. Clauser, F.H. - "Turbulent Boundary Layers in Adverse Pressure Gradients" - J. Aero. Sciences, Vol. 21,pp. 91-108, 1954.

23. Leutheusser, H.J. - "Turbulent Flow in Rectangular Ducts" - ASCE, J. of Hydraulics Div., Vol. 89, HY3, 1963.

24. Brundrett, E. and Baines, W.D. - "The Production and Diffusion of Vorticity in Duct Flow" - J. Fl. Mechanics, Vol. 19, Part 3, pp 375-392, 1964.

25. Itō, H. - "Friction Factors for Turbulent Flow in Curved Pipes" Trans. ASME, J. of Basic Engrg., Vol. 81, pp 123-134, June 1959.

APPENDIX A - Further Details of Apparatus

A.1 Steady Flow Conditions

Large scale fluctuations in the mean velocity especially for low air flow rates ($\bar{U} \cong 33$ ft/sec) and occurring at the rotational frequency were noticed and recorded on a Sandborn recorder. The introduction of the piece of honeycomb in the guide duct entrance reduced these from $\pm$ 5% to $\pm$ 2% in the worst cases. These fluctuations were still noticed during u' measurements at low air flow rates and rendered these measurements useless, but were not noticeable at high air flow rates ($\bar{U} = 60$ ft/sec).

A.2 Bulk Mean Velocity

The present tests were designed to measure differences in duct flows due to rotation alone. It was therefore of great importance that the bulk flow rate be kept constant and be accurately measurable and repeatable. Stationary and rotating inlet velocity profiles both on and off the centerline (Fig.21) showed that the Pitot-static tube gave an accurate measure of the bulk velocity when combined with the corrections

$\bar{U} = 0.95 \quad U_{\text{pitot-static}}$ for A.R. = 4:1, 7 1/3:1

$\bar{U} = 0.925 \quad U_{\text{pitot-static}}$ for A.R. = 1/2:1, 1:1

The bleeding in the air supply was used to maintain the pitot-static reading constant throughout a series of tests, and trial-and-error adjustment was necessary to allow for the centrifugal pumping performed by the apparatus.

A.3 Calibration of Transducer

A closely linear calibration curve (Fig.22) was obtained by comparing the amplified signals of the transducer with the readings of an inclined

Meriam manometer and a micrometer. The transducer was noticed to exhibit an interesting hysteresis effect dependent upon which side of the diaphragm the higher pressure was applied. This gave no problems, however, if when applying the pressure difference the higher pressure was connected first and when removing the pressure connections the lower pressure was the first to be removed. The transducer zeroing for no pressure difference was frequently checked.

APPENDIX B - Eddy Viscosity

B.1. Further Estimates of Eddy Viscosity

An inconsistency arises from the use of a constant eddy viscosity and the measured turbulent velocity profile in the solution of equation (12) from the axial velocity u_o. The calculation using the measured static-pressure gradient will give a parabolic profile even when the slip velocity is used for a boundary condition. Thus two attempts were made to match the velocity distribution with the eddy viscosity.

In the first method, the measured centerline velocity profile was taken from rotational tests and an attempt made to calculate the centerline eddy viscosity directly for the rotating duct. This method used the x-direction equation of motion without assuming secondary velocities and their derivatives to be negligible, i.e.

$$v \frac{\partial u}{\partial y} = 2\omega v - \frac{\partial \Phi}{\partial x} + \nu \nabla^2 u + \frac{\partial u}{\partial y} \frac{\partial \nu}{\partial y} \qquad \text{(B-1)}$$

Although v could be approximated by the calculations using ν = constant, and the velocity distribution u on the y-centerline along with the axial static pressure gradient were measured quantities, this method is critically dependent on a knowledge of $\frac{\partial^2 u}{\partial z^2}$. Figures 5 and 7 show that the term $\frac{\partial^2 u}{\partial y^2}$ is negligibly small in the middle of the channel for both the 1:1 and 1/2:1 aspect ratios. The magnitude of $\frac{\partial^2 u}{\partial z^2}$ in the non-rotating channel is not known with great precision, and when the velocity distribution has been modified by rotation the problem becomes impossible (unless the new distribution is measured for the complete duct).

An alternative method uses equation (12) modified to account for

variable viscosity.

$$\nabla\Phi = \nu\nabla^2 u + \frac{\partial u}{\partial y}\frac{\partial \nu}{\partial y} + \frac{\partial u}{\partial z}\frac{\partial \nu}{\partial z} \qquad \text{(B-2)}$$

The method relies on the assumption that the eddy viscosity is isotropic and independent of rotation.

A finite difference solution was obtained for equation (B-2) applied to the 3/4" square duct and the centerline values are shown in Figure 23. The boundary condition of $\nu = 0$ at the walls was chosen and the similarity assumption of equation (17) was used for the velocity distribution. A striking feature of the results is the small variation over most of the duct centerline where the assumed velocity is most accurate, although gradients in the viscosity appear important. The estimated value obtained from equation (18) is in remarkably close agreement.

The vastly simplifying assumption of small changes in eddy viscosity leads immediately to the calculation of the secondary axial velocity using the new eddy viscosity.

B.2 Isotropic Eddy Viscosity

The defining relations

$$\nu_{xy} = \frac{-\overline{u'v'}}{\partial u/\partial y}$$

$$\nu_{yz} = \frac{-\overline{v'w'}}{\frac{\partial v}{\partial z} + \frac{\partial w}{\partial y}} \qquad \text{(B-3)}$$

$$\nu_{xz} = \frac{-\overline{u'w'}}{\partial u/\partial z}$$

were used with the tabulated shear stresses and velocities of Brundrett and Baines[24] to calculate the three eddy viscosities for fully-developed

flow in a square channel. The values are shown in Table 4 and the centerline distribution of ν_{xy} is plotted in Figure 24.

Comparison of the eddy viscosities shows quite close agreement between ν_{xy} and ν_{xz}, while the values of ν_{yz} are especially good considering their dependence on the gradients of the secondary velocities v and w which are very difficult to measure. The calculated values of eddy viscosity obtained from equation (18) and from the procedure outlined in Section B.1 are in good agreement with each other but are a factor of three smaller than the measured values.

APPENDIX C - Frictional Pressure Drop

C.1. Standstill Tests

The measured static pressure gradient based on the pressure drop between duct stations x = 6 inches and x = 54 inches was compared with that predicted by the Blasius formula using the hydraulic mean diameter

$$f_s = 0.316 \left(\frac{\rho \bar{U} d_h}{\mu}\right)^{-1/4} \qquad \text{(C-1)}$$

where

$$f = \frac{\frac{dp}{dx} dy}{\frac{1}{2} \bar{U}^2} \qquad \text{(C-2)}$$

The mean velocity $\bar{U}$ was obtained from the inlet pitot-static tube (discussed in Appendix A.2) and gave results which agreed within 10%, the experimental values being generally smaller. The friction factors for no rotation are shown in Figure 25 compared with equation (C-1).

C.2. Rotating Tests

The friction factors calculated from equation (C-2) are shown in Table 3 and the non-dimensional values f_R/f_s are plotted in Figure 26. The friction factors generally increased with rotation, the largest increases being at the 1:1 aspect ratio.

Trefethen[1] has pointed out the analogy which to a first approximation exists between the fluid flow in rotating, bent and heated horizontal tubes. Further he has shown that the secondary flow effects in both turbulent and laminar flow can be closely approximated as independent of the nature of the transverse body force. It was also suggested that the kind of secondary flow and its effects on the friction

factor are determined by the magnitude of the total transverse body force, as well as the duct size and geometry, and the fluid properties. An estimate of the transverse body force can be obtained by assuming all the fluid moves with its mean velocity $\bar{U}$ which leads to the conclusion that the same functional form will relate $f_c(N/n_o)^{1/2}$ to $R_{e_L}(n_o/N)^2$ in bent ducts as relates $f_R/(\omega 2n_o/\bar{U})^{1/2}$ to $R_{e_L}(\omega 2n_o/\bar{U})^2$ in rotating ducts.

Ito[25] has suggested the following empirical formula for the friction factor in bent pipes

$$f_c \left(\frac{N}{n_o}\right)^{1/2} = \frac{0.316}{[R_{e_L}(n_o/N)^2]^{1/2}} \qquad \text{(C-3)}$$

This relation applies for values of the parameter $R_{e_L}(n_o/N)^2$ greater than 6, and by use of the Blasius friction formula, equation (C-1), equation (C-3) becomes

$$\frac{f_c}{f_s} = 1.00\,[R_{e_L}(n_o/N)^2]^{1/20} \qquad \text{(C-4)}$$

If the Blasius formula and the concept of hydraulic diameter are taken as applying to rectangular ducts, and the analogy with rotating pipes is used, equation (C-4) becomes

$$\frac{f_R}{f_s} = [R_{e_L}(\omega d_h/\bar{U})^2]^{1/20} \qquad \text{(C-5)}$$

This relation was used to estimate the effects of rotation on the friction factor in the present tests and the comparison is shown in Figure 26. Very close agreement is noticed for the 1:1 aspect ratio while the

calculated values are consistently high for the other aspect ratios. The maximum measured change for the spin rates used was only 20% and most of the results were within experimental accuracy, thus the present experiments did not provide a significant test of the theory. It appears that the hydraulic mean diameter may have limited success in this application.

In a more recent paper Trefethen[2] has presented the results of a series of tests designed to measure the effects of rotation on turbulent flow in circular pipes. These tests were performed at various Reynolds' numbers (R_{e_L}) and those results with R_{e_L} close to the present experimental values are plotted with the 1:1 (square duct) data in Figure 27. Also plotted are the variations predicted using equation (C-5). The agreement is seen to be very good although the changes were at maximum only 20% with the experimental accuracy within 10%. The calculation of secondary axial velocities (see Section III F) did give a positive value of C_2 (i.e. an increase in friction factor) in its range of applicability, but this range was not extensive enough for comparison here.

TABLE 3 MEASURED VALUES OF SKIN FRICTION, MOMENTUM PARAMETER AND FRICTION FACTOR

SPIN PARAMETER $\frac{\omega D}{\bar{U}}$	PRESTON TUBE SKIN FRICTION C_{f_P}	PRESTON TUBE SKIN FRICTION C_{f_S}	CLAUSER SKIN FRICTION C_{f_P}	CLAUSER SKIN FRICTION C_{f_S}	MOMENTUM PARAMETER ξ	FRICTION FACTOR f
ASPECT RATIO = $\frac{1}{2}$: 1, $Re_L = 2.80 \times 10^4$, $\bar{U}$ = 54.5 Ft/Sec, U = 63.4 Ft/Sec						
.0	.00570	.00570	.00585	.00585	.0	.0224
.0076	.00640	.00513	.00650	.00493	.00272	.0226
.0163	.00801	.00355	.00800	.00384	.01738	.0229
.0244	.00822	.00295	.00832	.00348	.02858	.0234
.0371	.00822	.00287	.00830	.00350	.03227	.0238
.0492	.00858	.00287	.00820	.00325	.03790	.0242
$\frac{1}{2}$: 1, 1.65×10^4, 32.1, 36.2						
.0	.00543	.00543	.00622	.00622	.0	.0246
.0163	.00750	.00315	.00793	.00420	.01512	.0251
.0408	.00875	.00211	.00931	.00358	.03535	.0261
.0610	.00922	.00164	.00993	.00362	.03624	.0274
.0820	.01020	.00129	.01060	.00362	.04287	.0279
1 : 1, 2.00×10^4, 51.2, 59.0						
.0	.00620	.00620	.00625	.00625	.0	.0230
.0039	.00675	.00538	.00672	.00565	.00214	.0233
.0076	.00748	.00453	.00750	.00471	.01161	.0242
.0117	.00770	.00420	.00772	.00440	.01711	.0244
.0163	.00757	.00371	.00767	.00422	.02112	.0247
.0207	.00760	.00357	.00781	.00340	.02538	.0253
.0240	.00787	.00333	.00796	.00386	.02566	.0262
1 : 1, 1.29×10^4, 33.8, 37.0						
.0	.00550	.00550	.00577	.00577	.0	.0251
.0076	.00647	.00375	.00750	.00480	.01030	.0267
.0244	.00787	.00280	.00836	.00384	.01659	.0273
.0355	.00880	.00375	.00935	.0 447	.02251	.0301

TABLE 3 (Cont.)

SPIN PARAMETER $\frac{\omega D}{\bar{U}}$	PRESTON TUBE SKIN FRICTION C_{f_P}	PRESTON TUBE SKIN FRICTION C_{f_S}	CLAUSER SKIN FRICTION C_{f_P}	CLAUSER SKIN FRICTION C_{f_S}	MOMENTUM PARAMETER ξ	FRICTION FACTOR f
ASPECT RATIO = 4 : 1, $Re_L = 3.50 \times 10^4$, $\bar{U}$ = 57.0 Ft/Sec, U = 67.0 Ft/Sec						
.0	.00635	.00627	.00640	.00640	.0	.0237
.0039	.00672	.00624	.00665	.00621	.00033	.0237
.0076	.00695	.00575	.00685	.00585	.00156	.0238
.0117	.00705	.00548	.00702	.00551	.00280	.0238
.0163	.00663	.00551	.00720	.00591	.00167	.0239
.0207	.00677	.00548	.00687	.00540	.00394	.0241
.0244	.00690	.00548	.00727	.00549	.00337	.0241
4 : 1, 2.04×10^4, 33.2, 38.4						
.0	.00663	.00663	.00710	.00710	.0	.0251
.0076	.00701	.00578	.00825	.00662	.00206	.0254
.0163	.00738	.00504	.00825	.00606	.00478	.0256
.0244	.00762	.00476	.00825	.00600	.00444	.0262
.0296	.00808	.00476	.00900	.00530	.00705	.0267
.0355	.00845	.00476	.00950	.00620	.00720	.0272
.0408	.00787	.00476	.00930	.00595	.00619	.0277
$7\frac{1}{3}$: 1, 3.85×10^4, 57.0, 66.3						
.0	.00636	.00650	.00634	.00634	.0	.0233
.0039	.00666	.00621	.00653	.00627	.00009	.0233
.0076	.00664	.00600	.00670	.00630	.00020	.0235
.0117	.00706	.00589	.00692	.00588	.00043	.0235
.0163	.00657	.00614	.00655	.00617	.00112	.0239
.0207	.00678	.00607	.00690	.00614	.00095	.0241
$7\frac{1}{3}$: 1, 2.24×10^4, 33.2, 38.3						
.0	.00627	.00627	.00720	.00720	.0	.0233
.0076	.00654	.00602	.00745	.00695	.00018	.0239
.0163	.00689	.00602	.00768	.00692	.00048	.0245
.0244	.00713	.00591	.00780	.00680	.00096	.0253
.0296	.00726	.00566	.00797	.00675	.00127	.0259
.0355	.00717	.00541	.00810	.00686	.00135	.0262

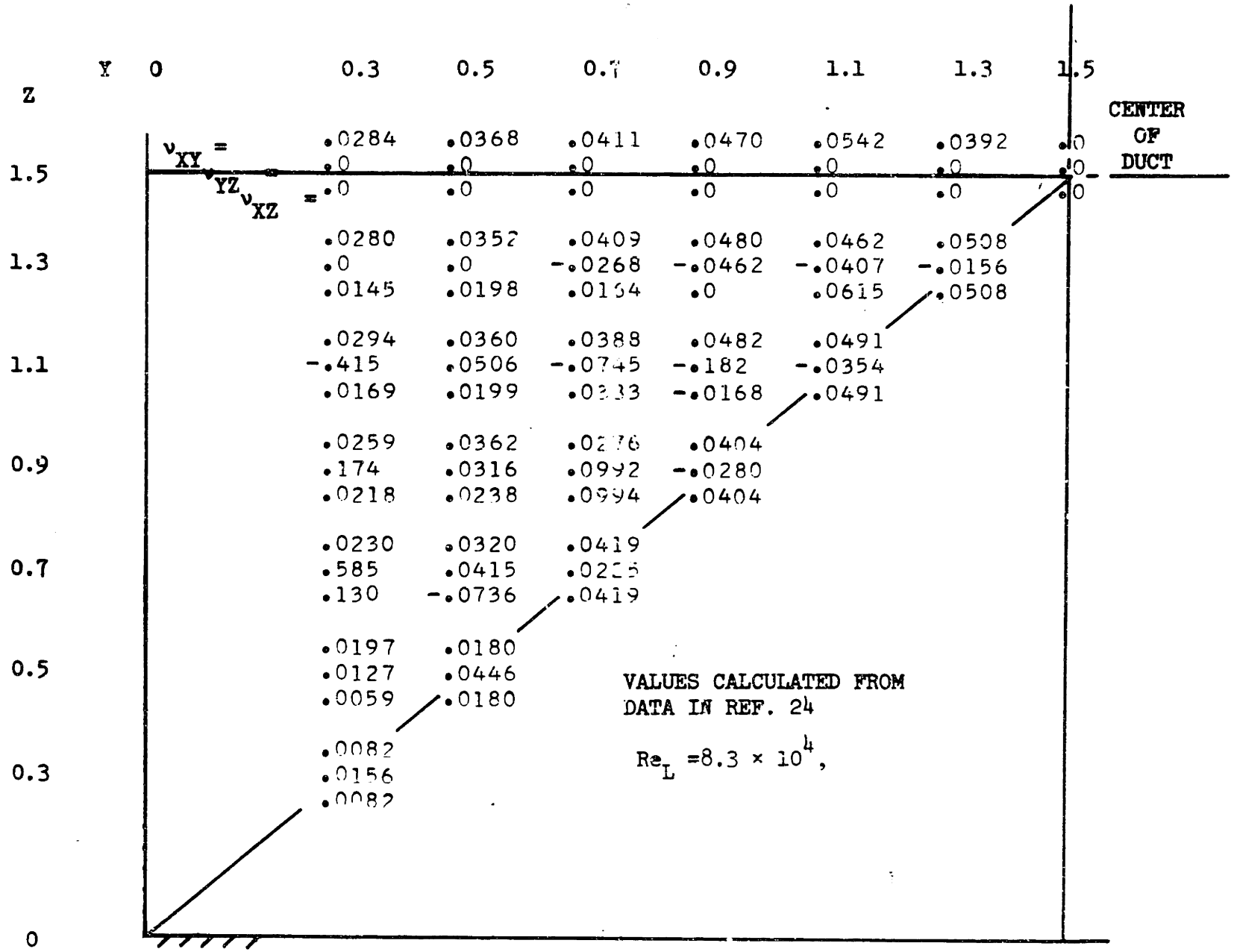

TABLE 4 EDDY VISCOSITIES FOR AN EIGHTH SEGMENT OF 3" SQUARE CHANNEL

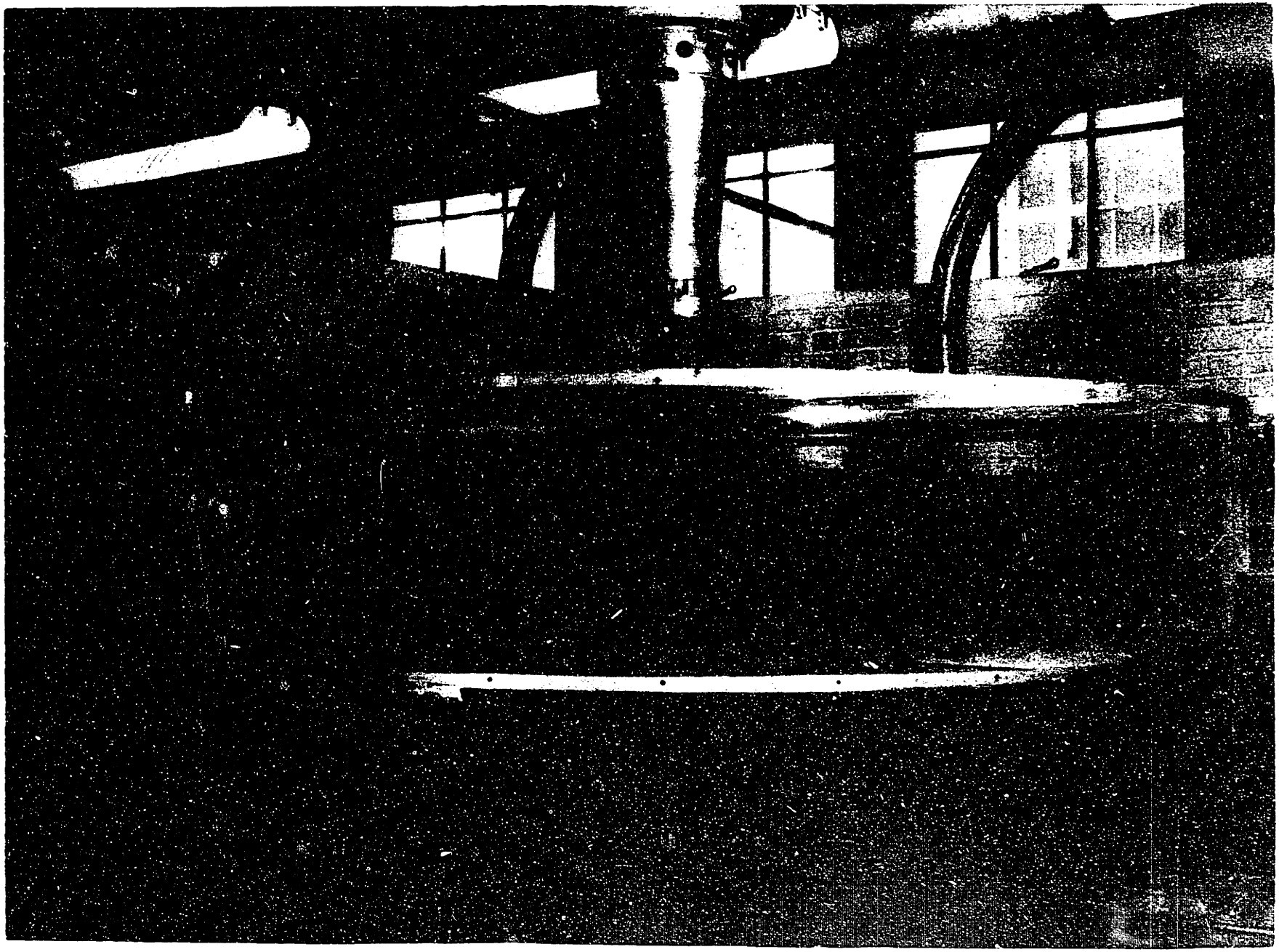

FIGURE 1a GENERAL VIEW OF TURNTABLE

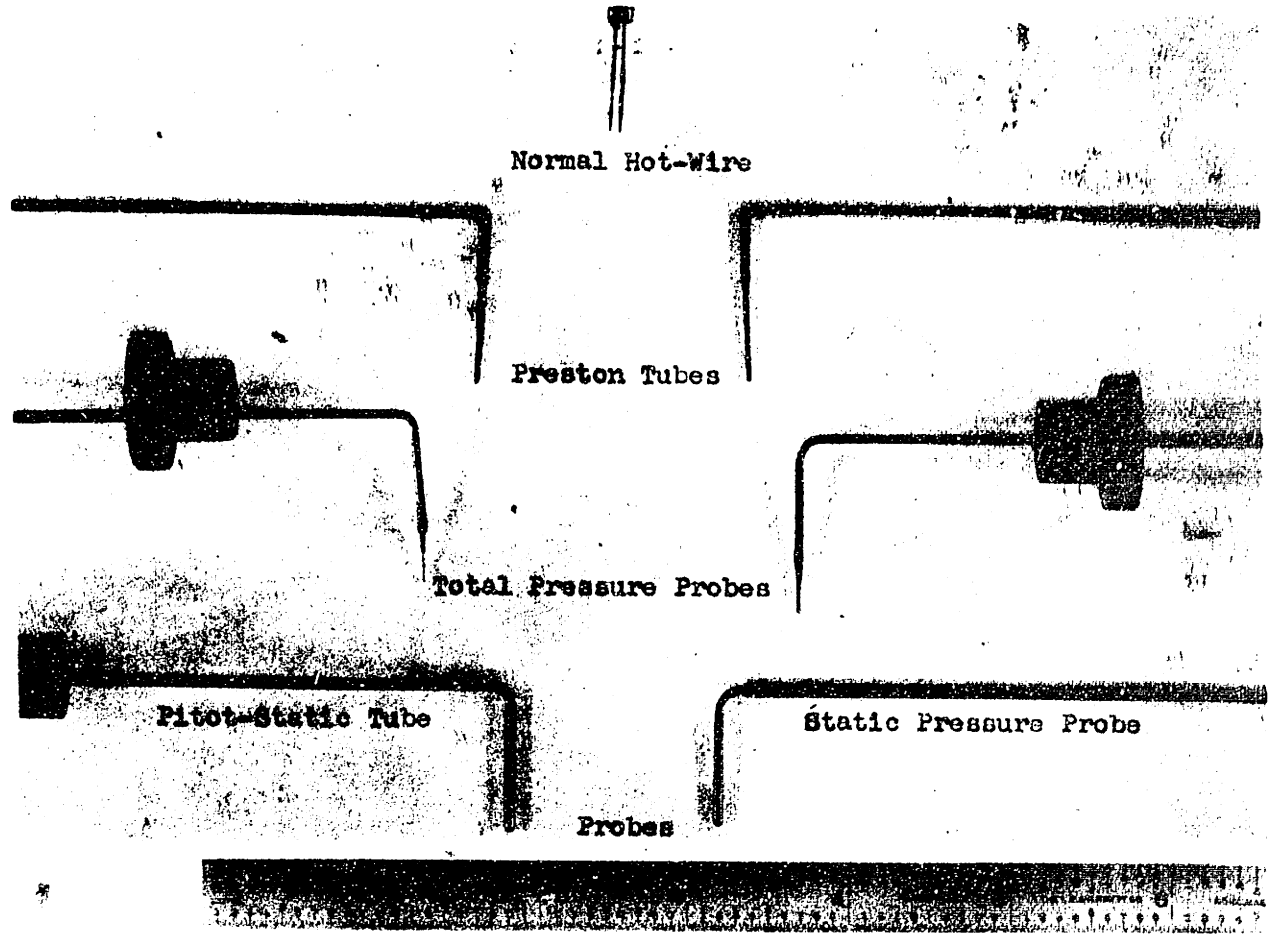

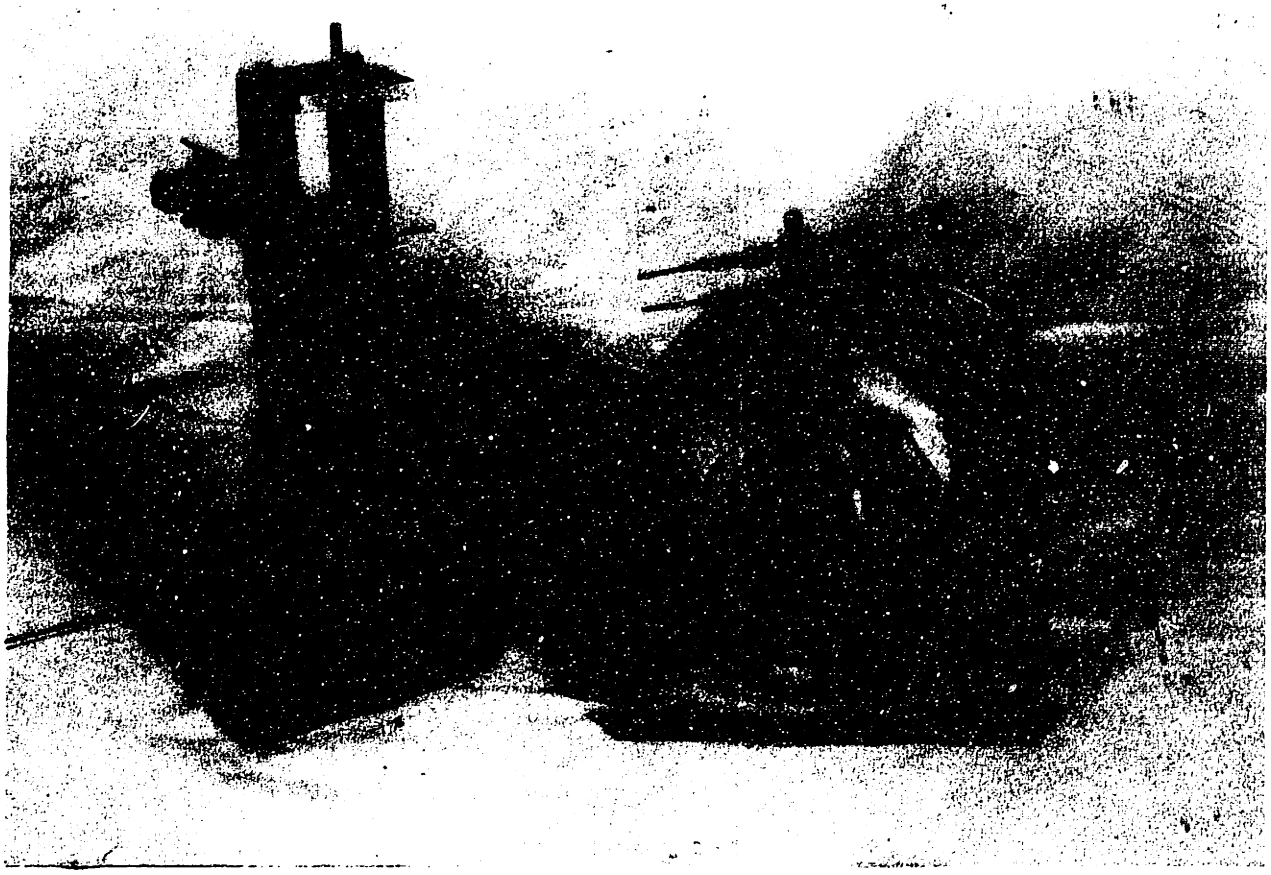

FIGURE 1b MEASURING PROBES; TRAVERSING MECHANISM, TRANSDUCER

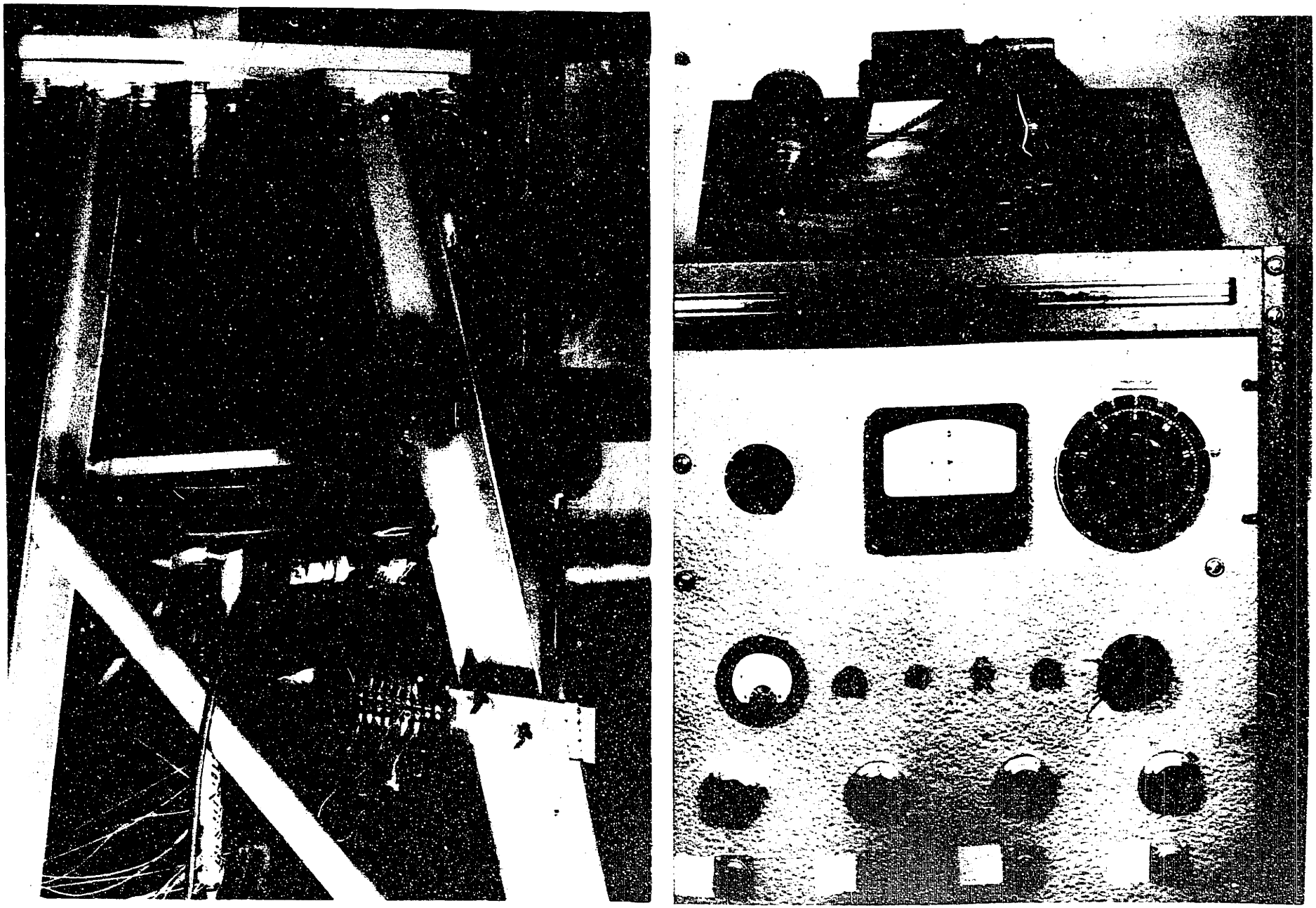

FIGURE 1c SLIP-RING PRESSURE TRANSMITTER, SLIP RINGS, TACHOMETER; AMPLIFIER and SELSYN GENERATOR

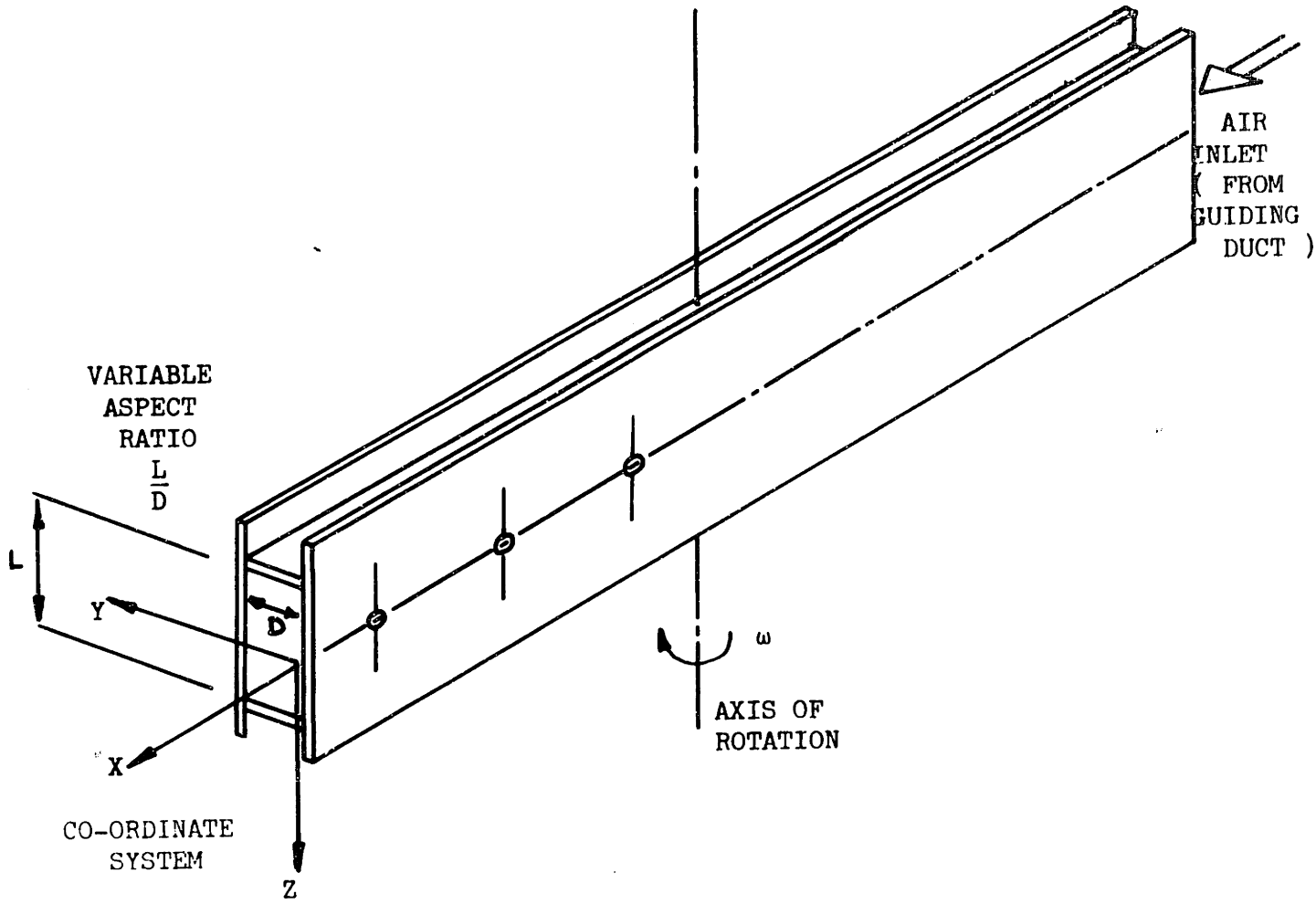

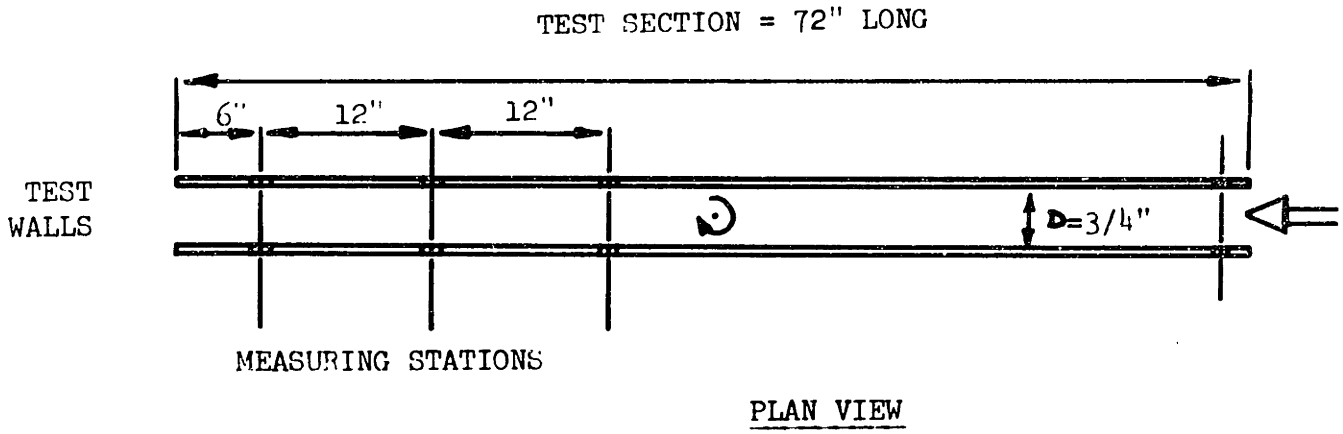

FIGURE 2 SCHEMATIC OF TEST SECTION

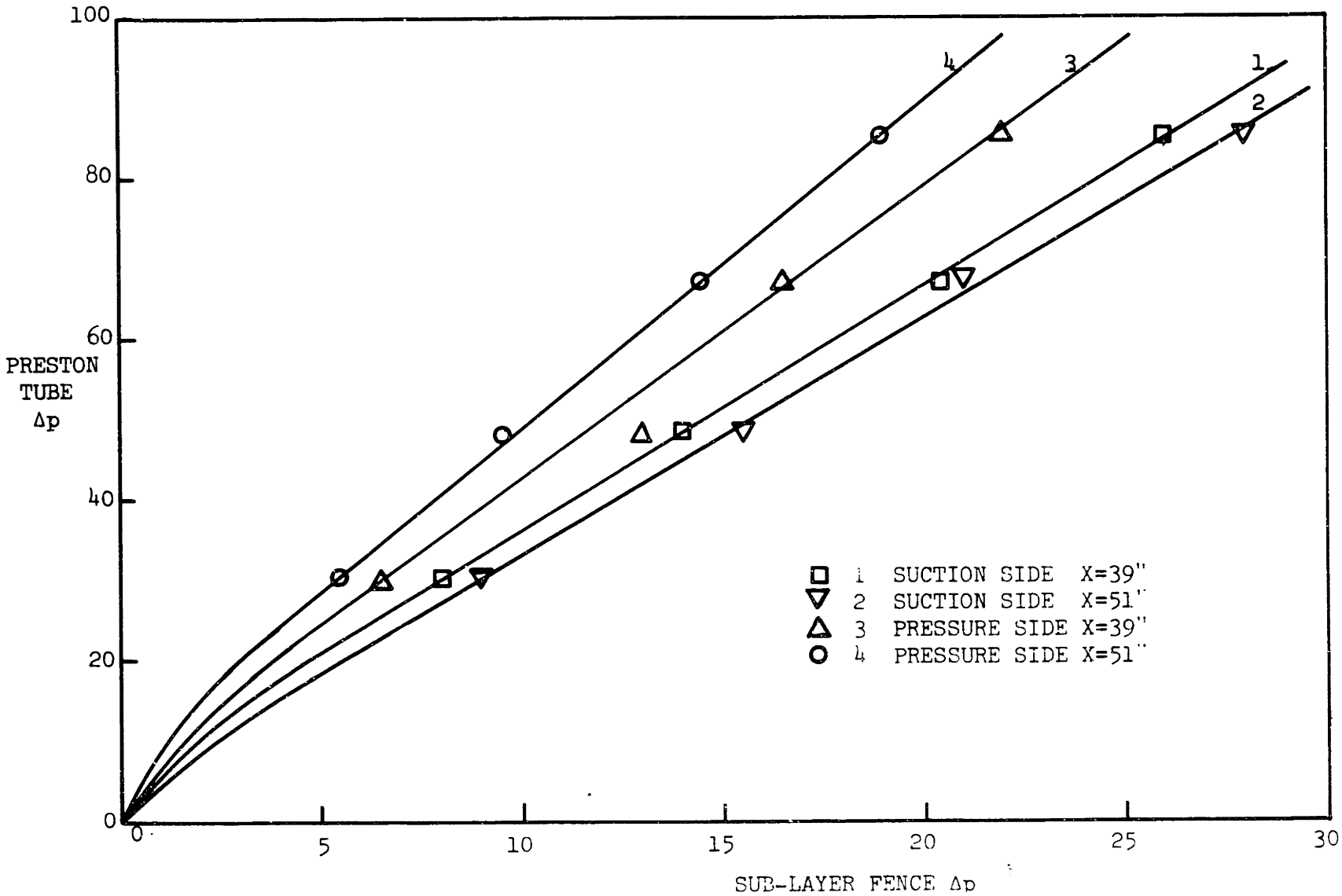

FIGURE 3 SUB-LAYER FENCE CALIBRATION CURVES

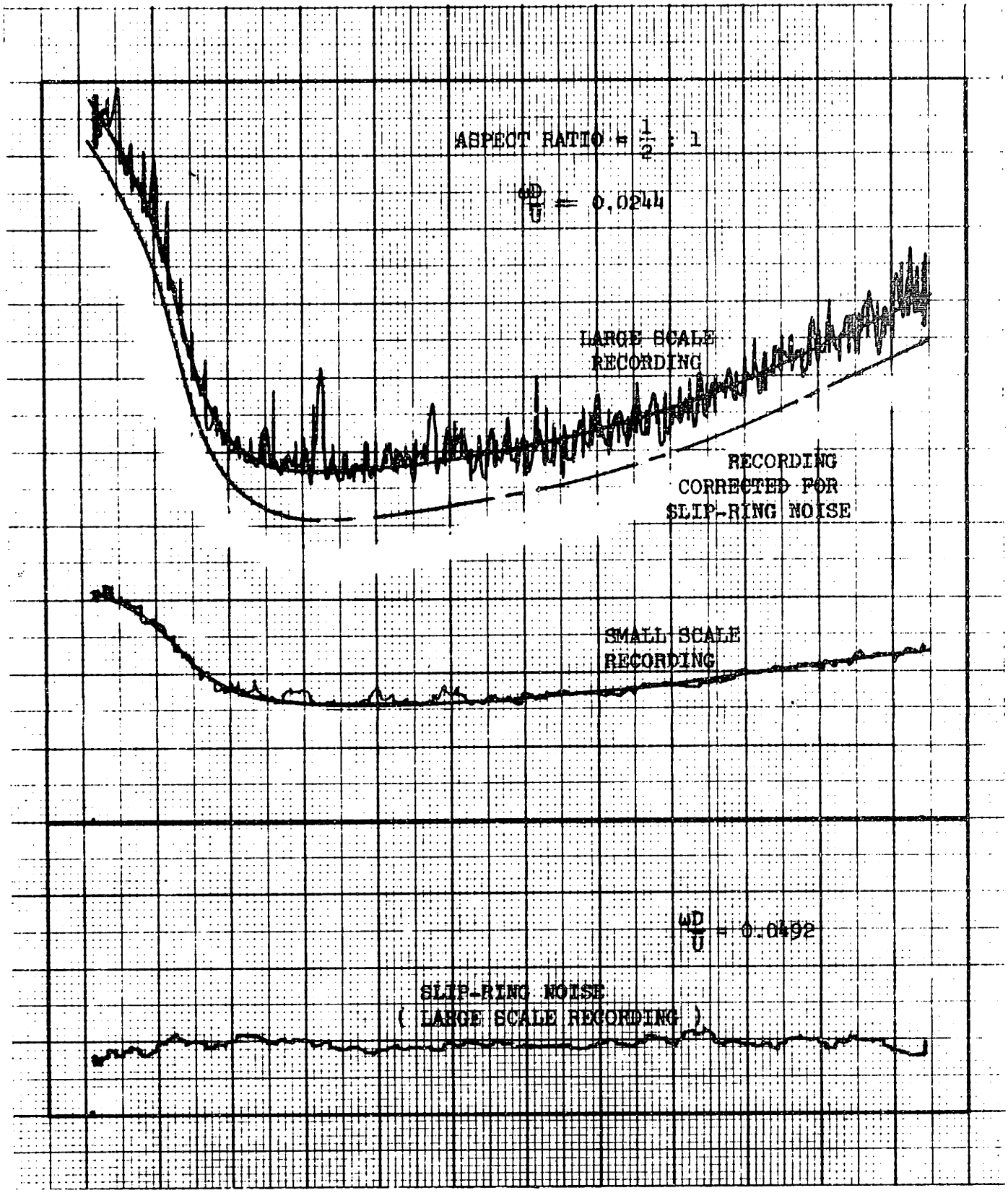

FIGURE 4 TYPICAL DATA AND REDUCTION PROCEDURE FOR u' TURBULENCE

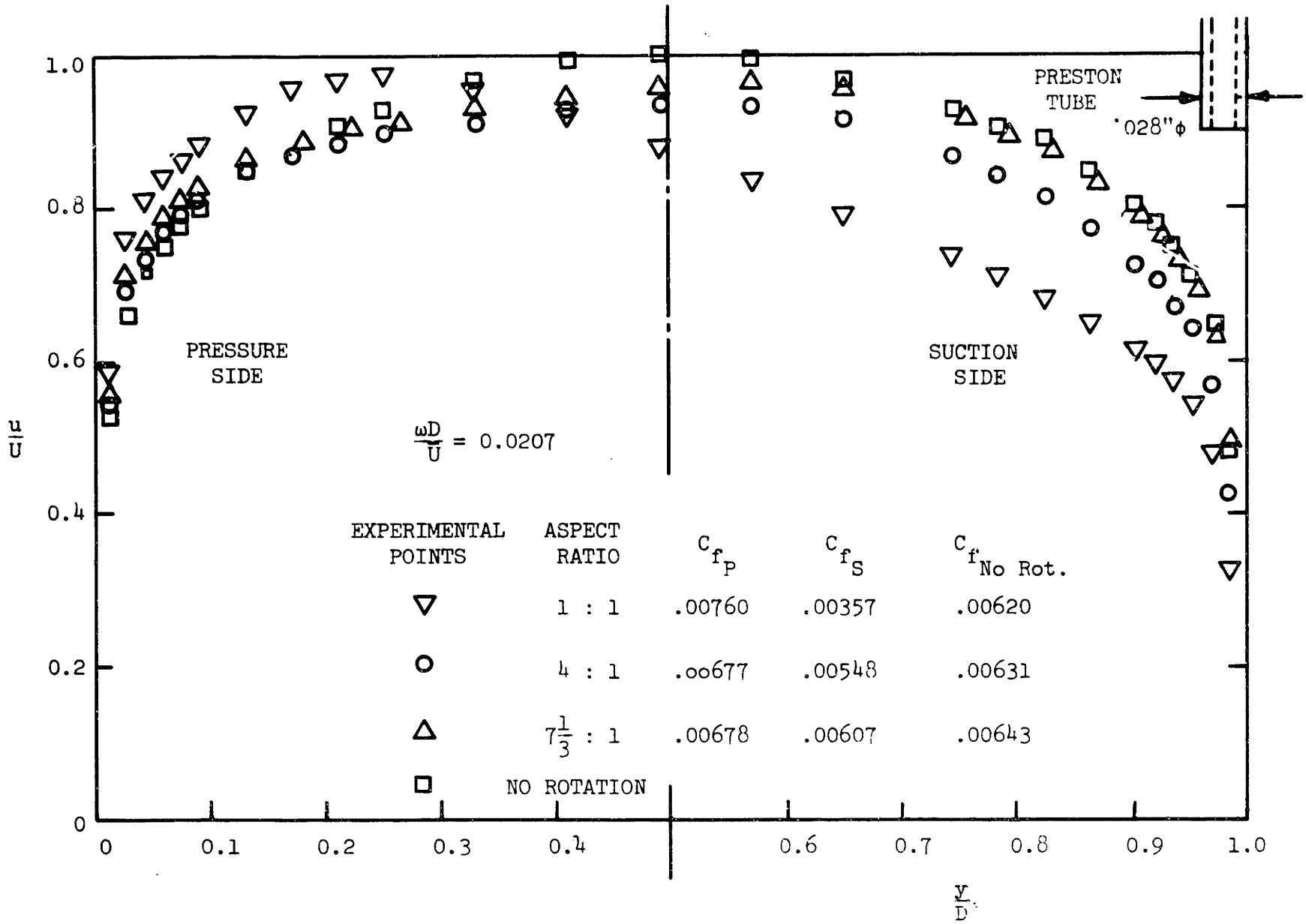

FIGURE 5 CENTERLINE VELOCITY PROFILES

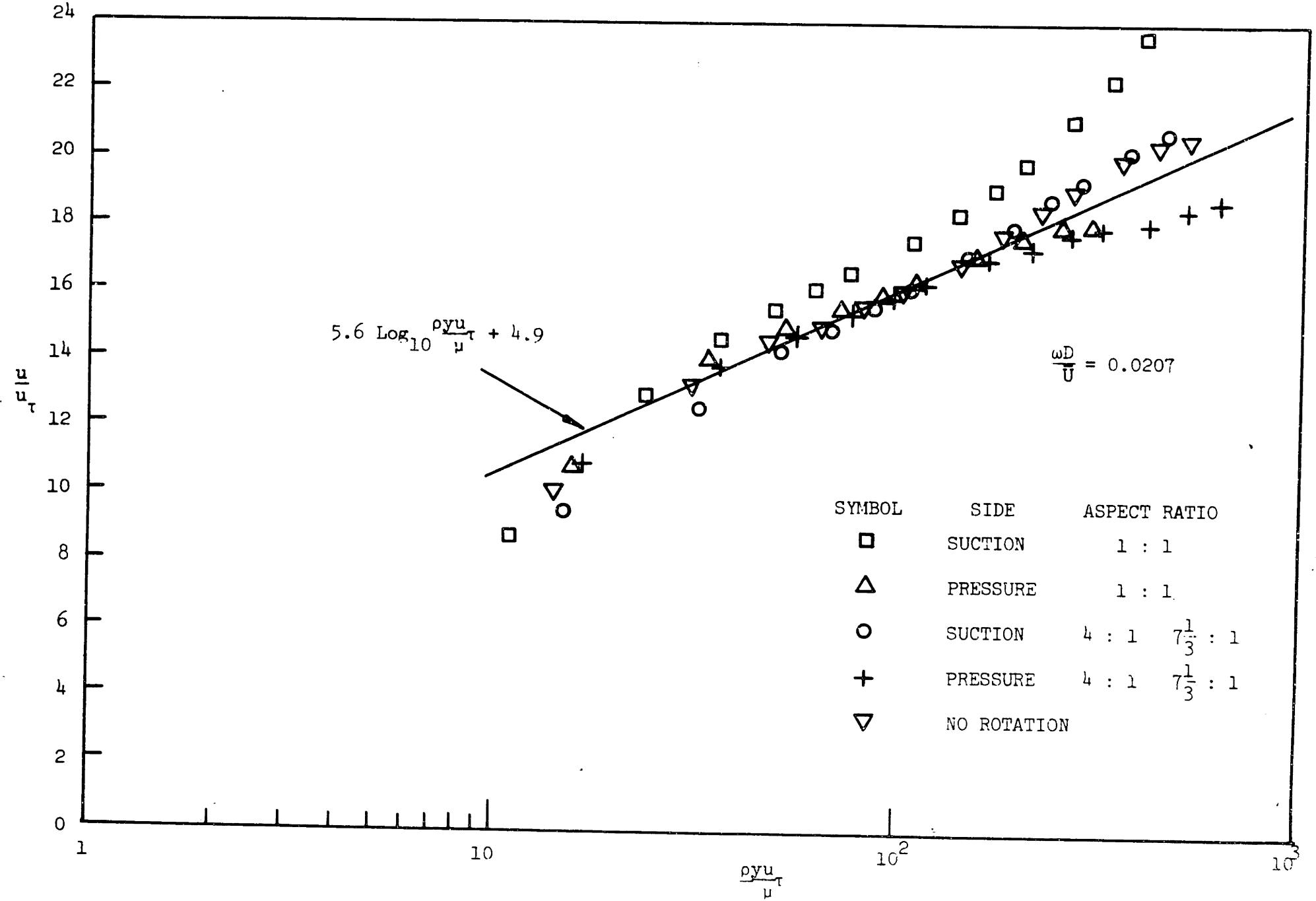

FIGURE 6 COMPARISON OF VELOCITY PROFILES WITH LAW OF THE WALL

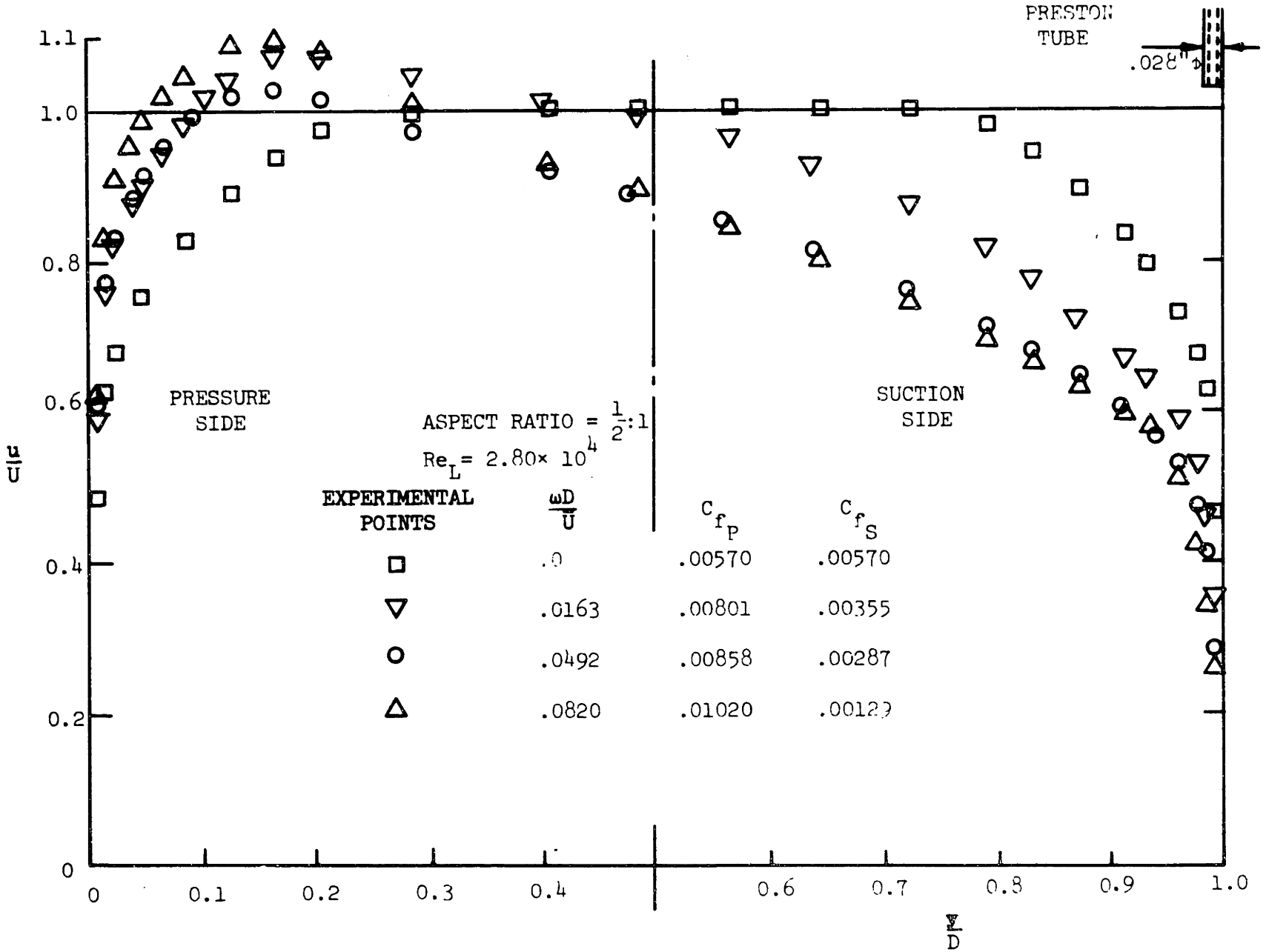

FIGURE 7 CENTERLINE VELOCITY PROFILES

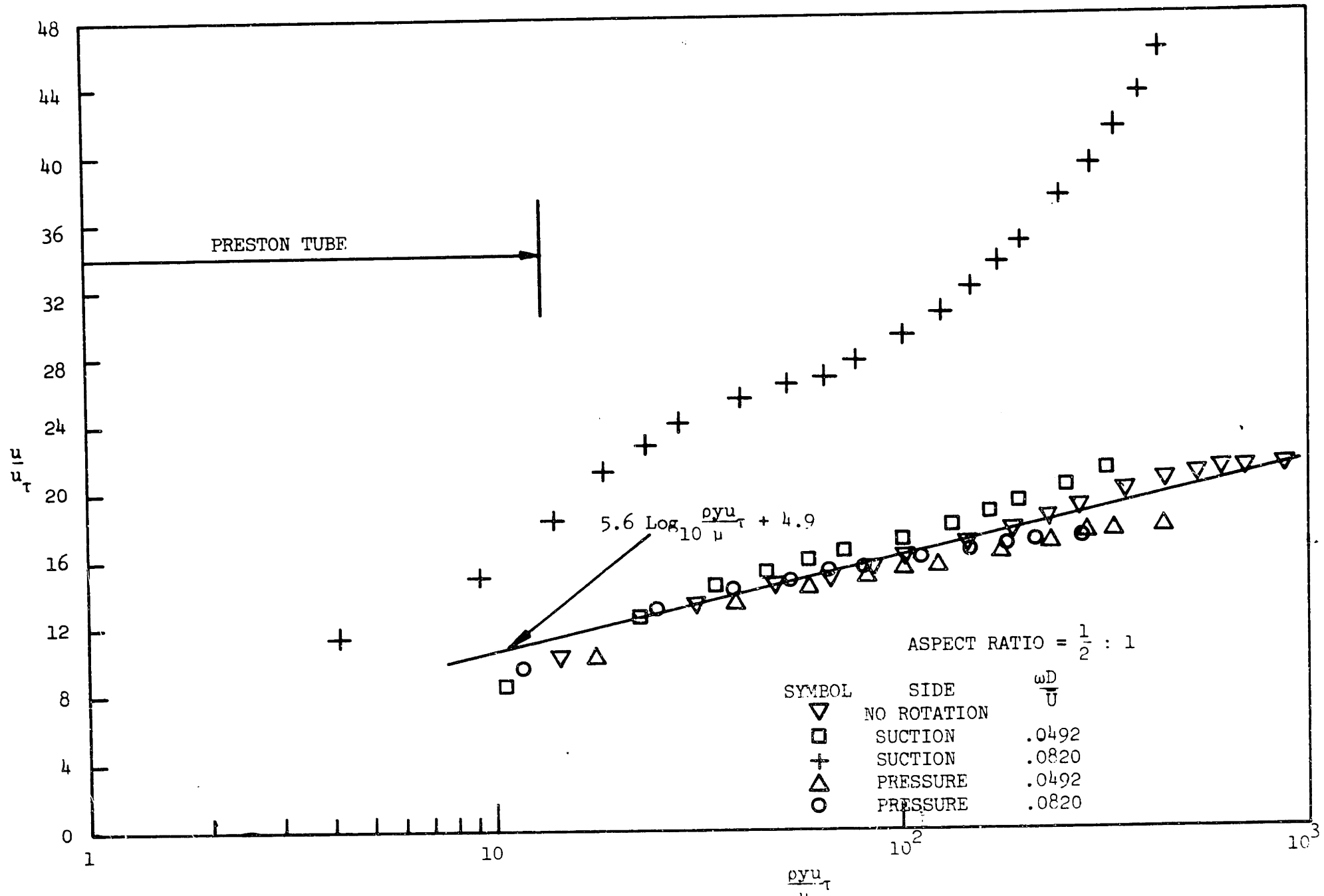

FIGURE 8 COMPARISON OF VELOCITY PROFILES WITH LAW OF THE WALL

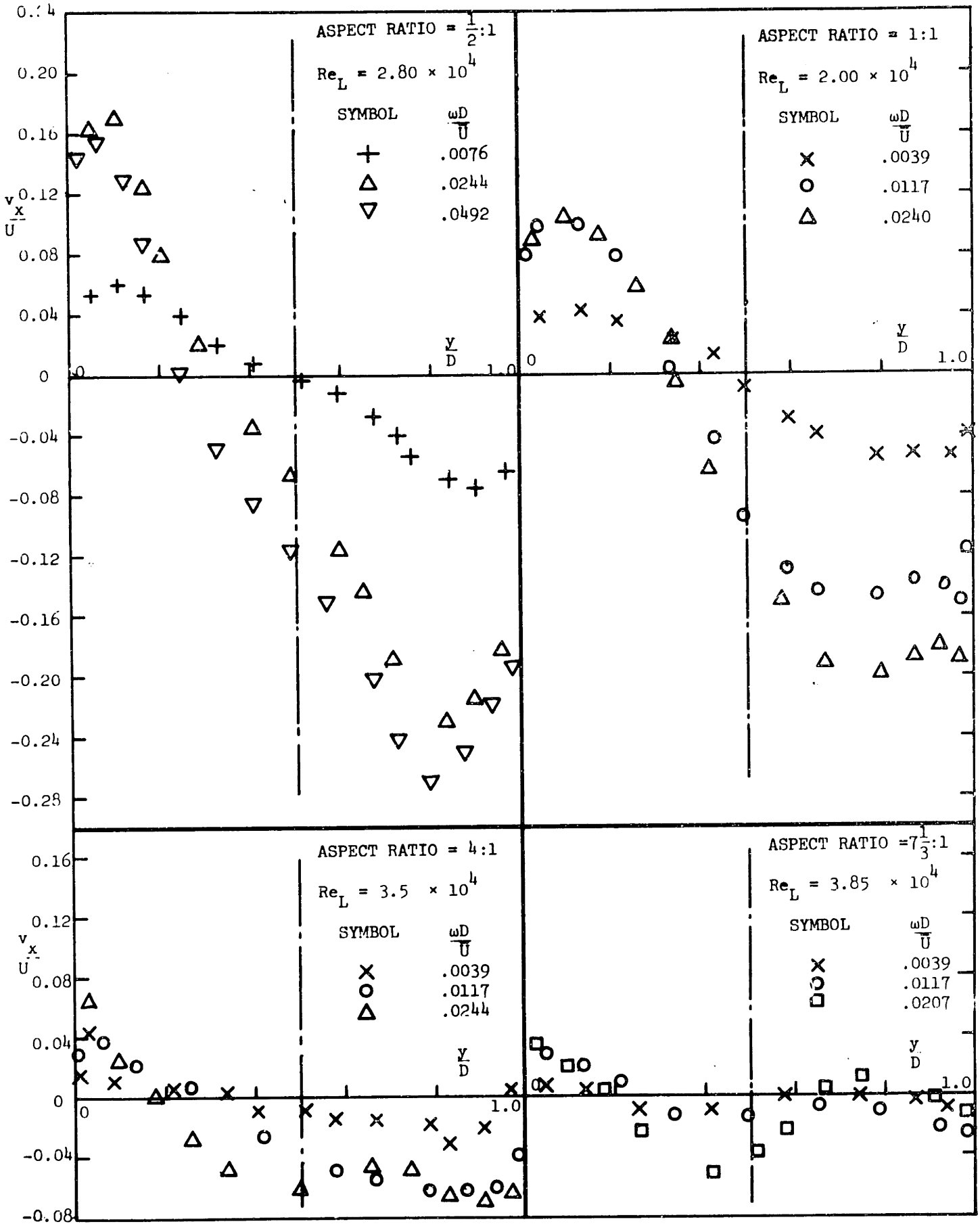

FIGURE 9 SECONDARY AXIAL VELOCITIES, HIGH Re_L

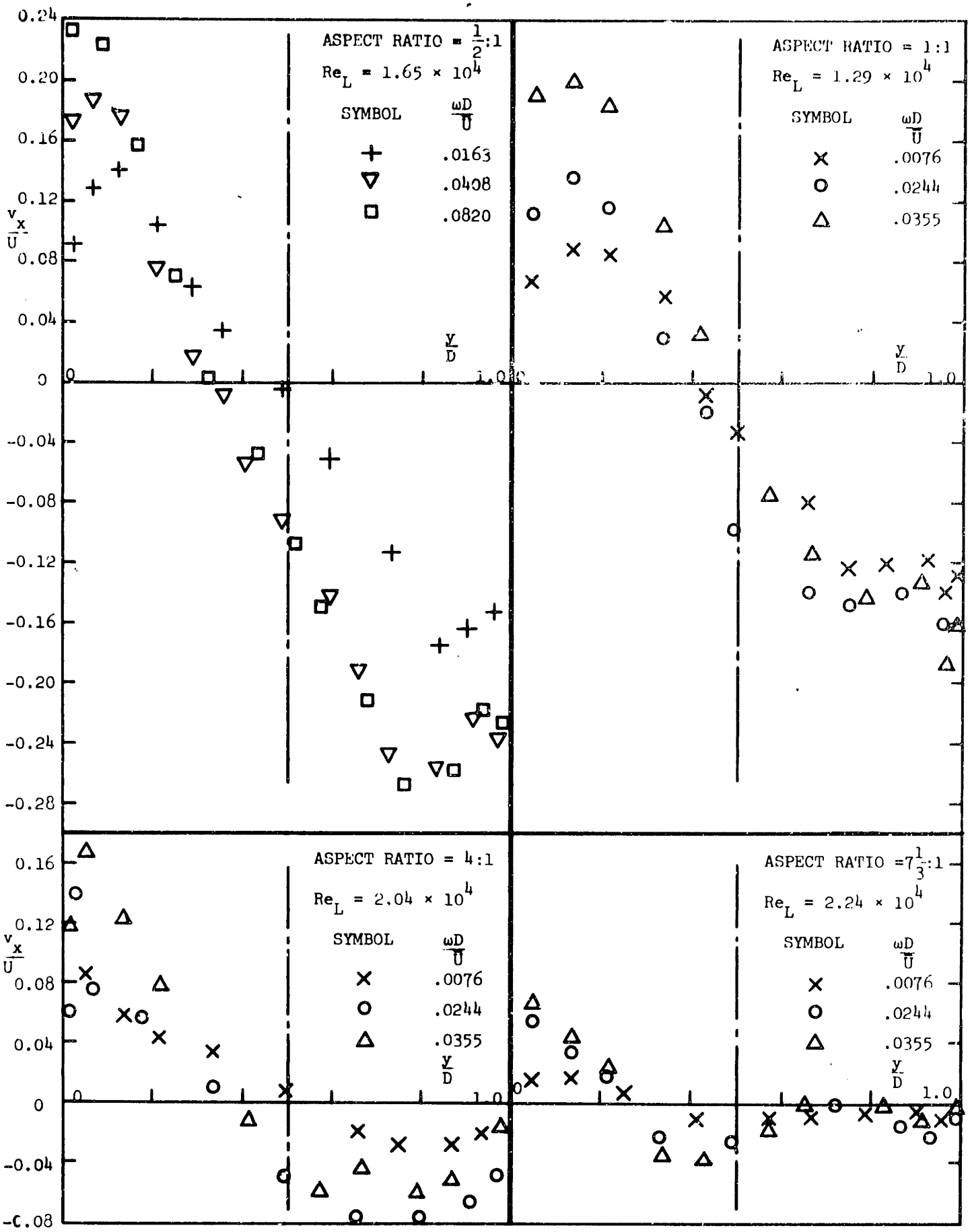

FIGURE 10 SECONDARY AXIAL VELOCITIES, LOW Re_L

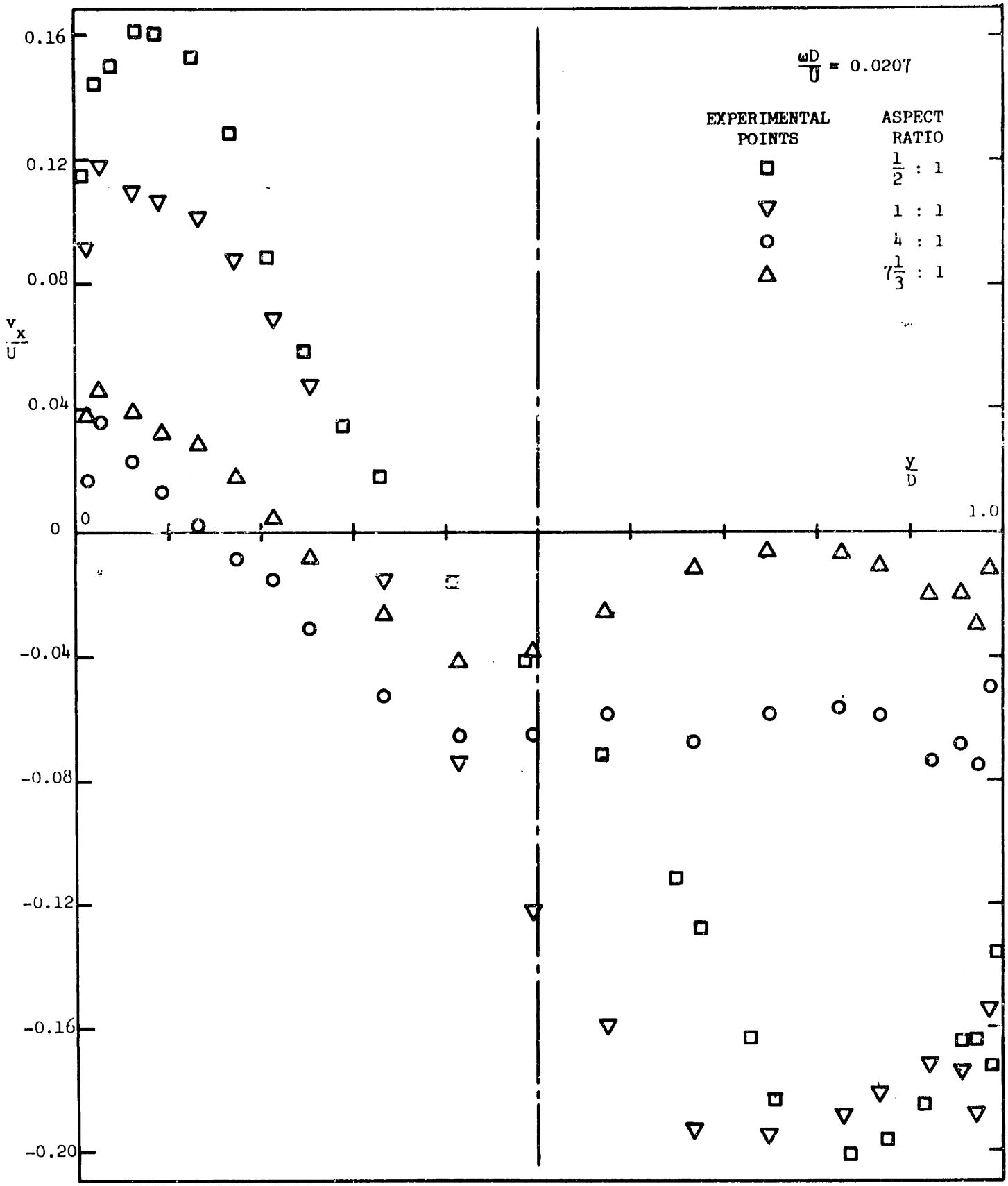

FIGURE 11 SECONDARY AXIAL VELOCITIES MEASURED ON CENTERLINE

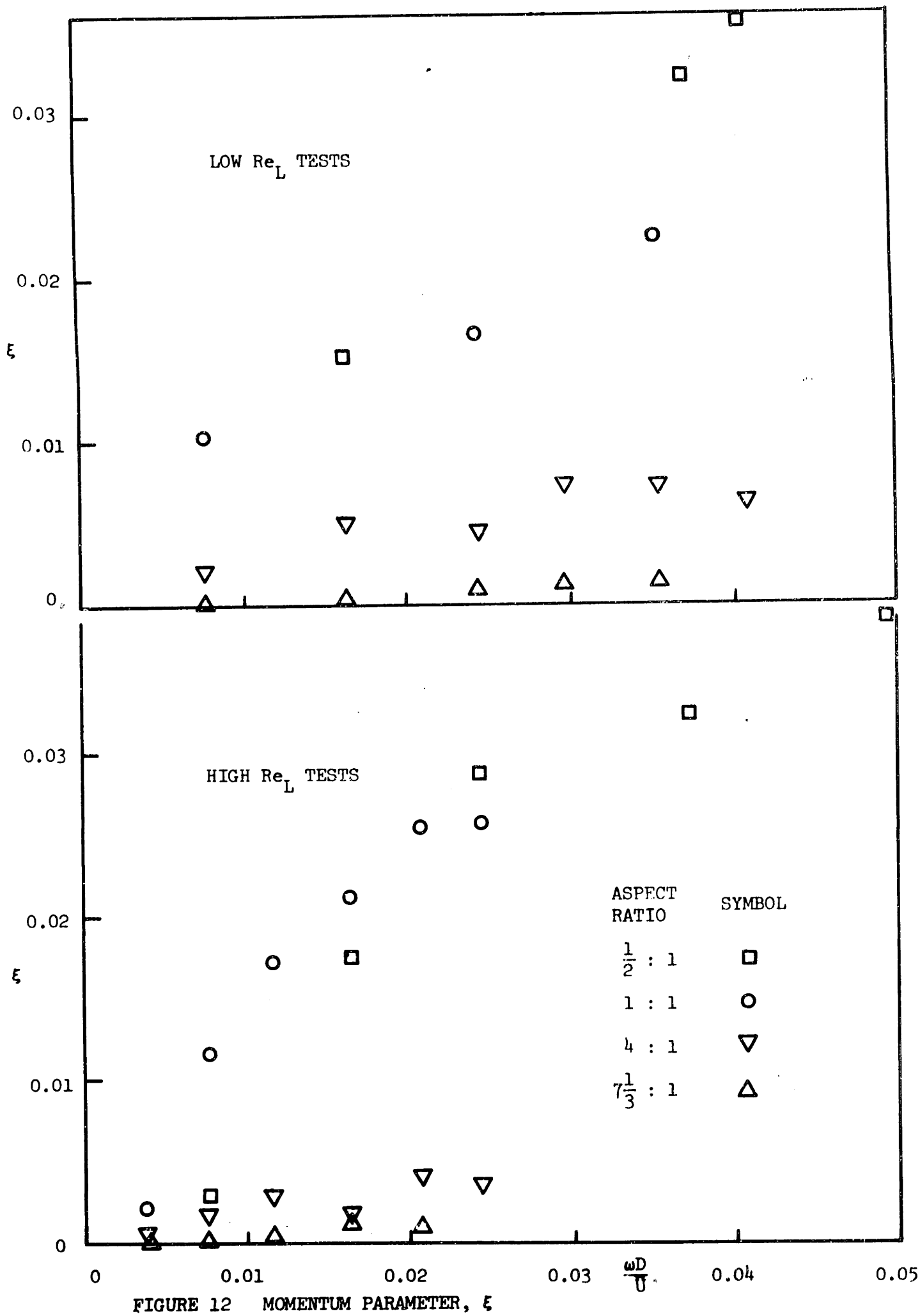

FIGURE 12 MOMENTUM PARAMETER, ξ

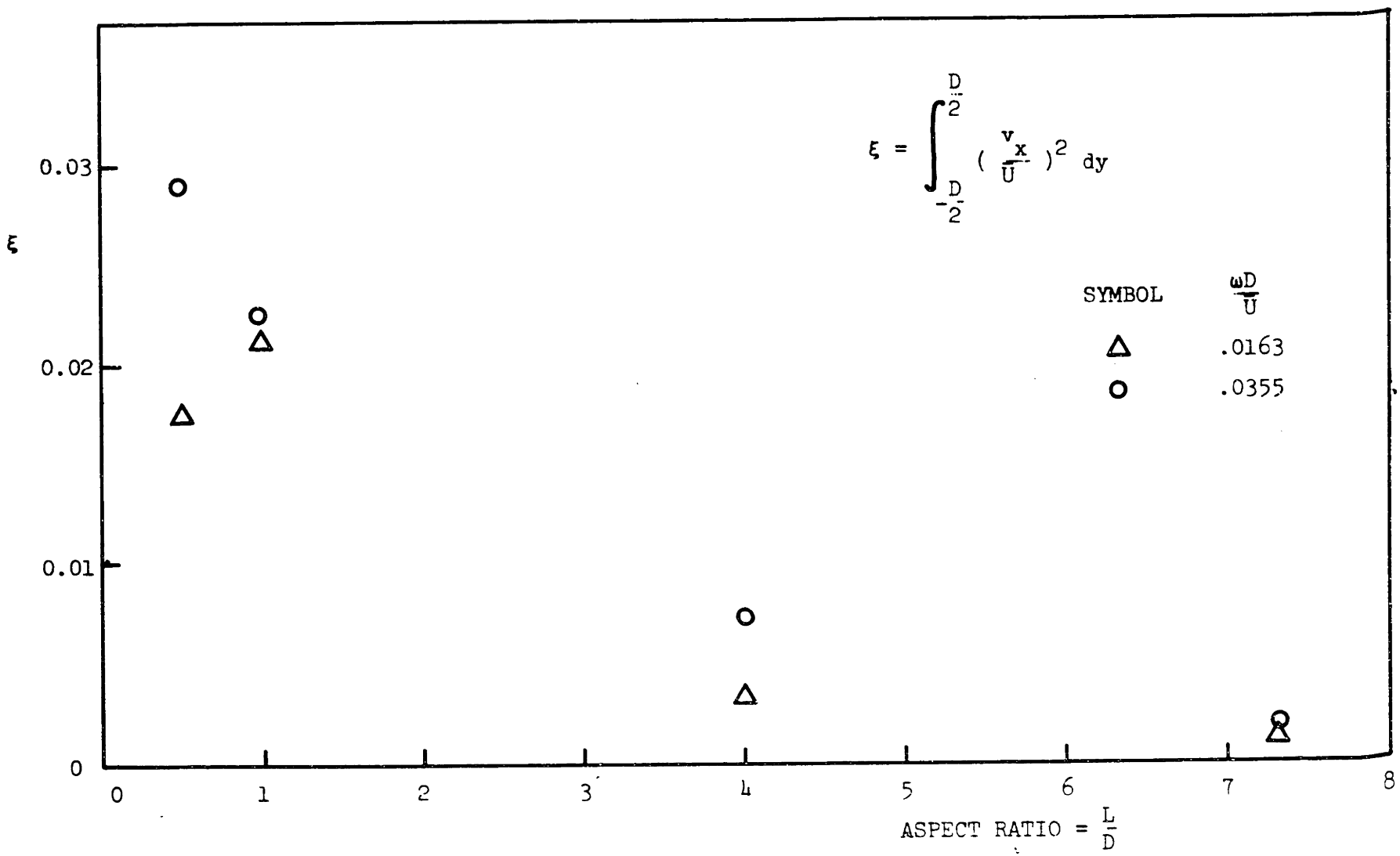

FIGURE 13 MOMENTUM PARAMETER, ξ, PLOTTED AGAINST ASPECT RATIO

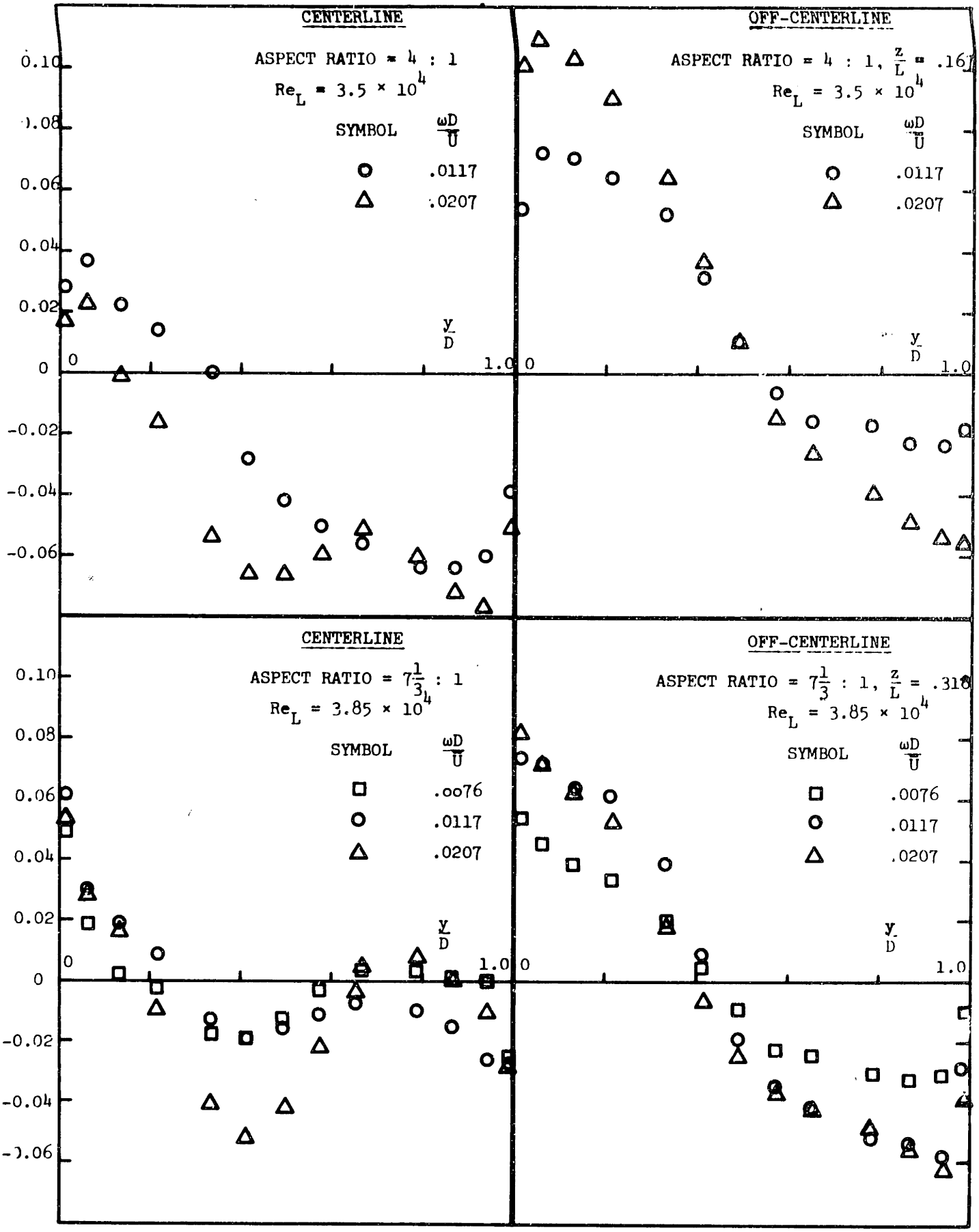

FIGURE 14 OFF- CENTERLINE VELOCITY PROFILES

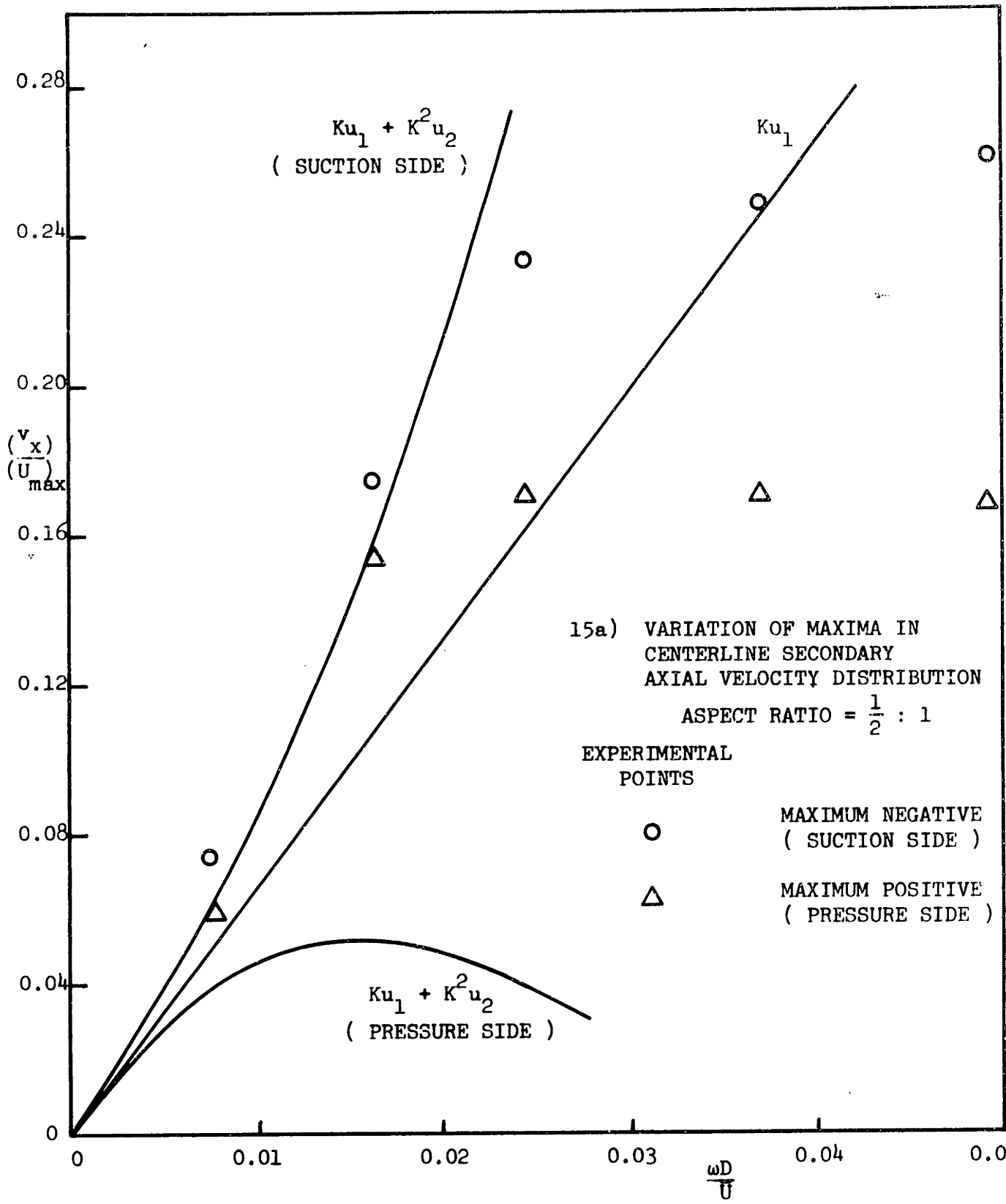

FIGURE 15 COMPARISON OF MEASURED AND CALCULATED SECONDARY AXIAL VELOCITIES

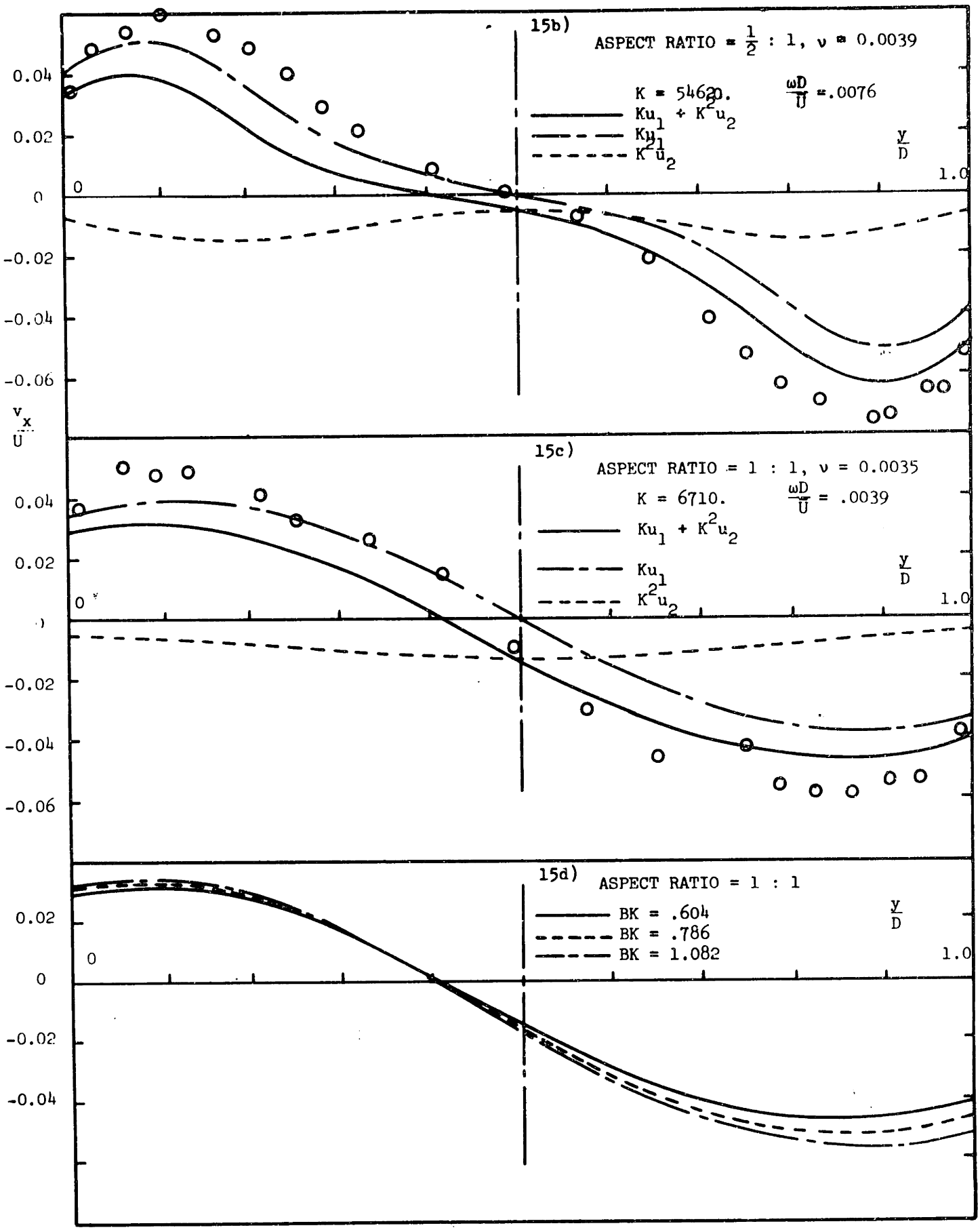

FIGURE 15 COMPARISON OF MEASURED AND CALCULATED SECONDARY AXIAL VELOCITIES

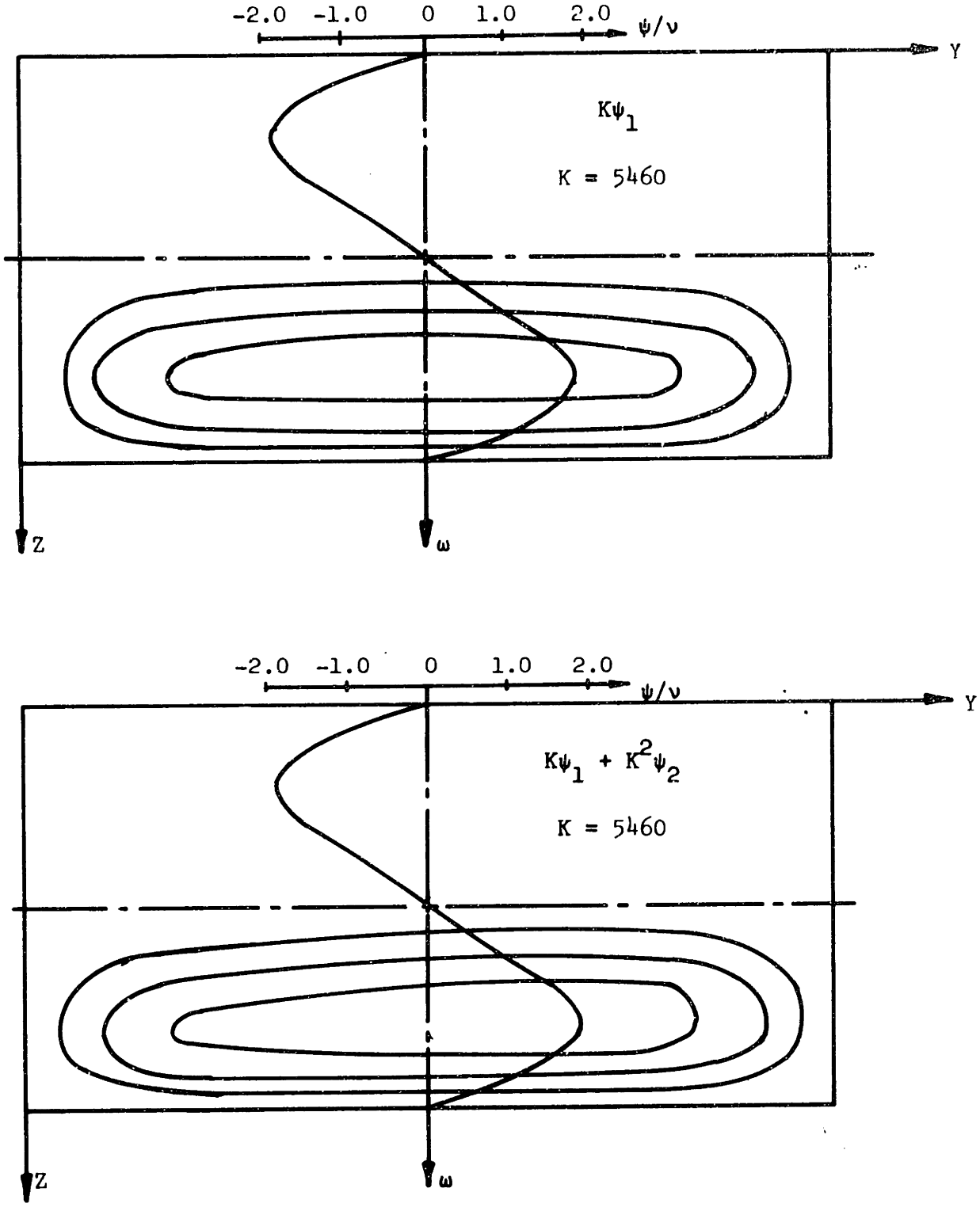

FIGURE 16 CALCULATED STREAM FUNCTION ψ

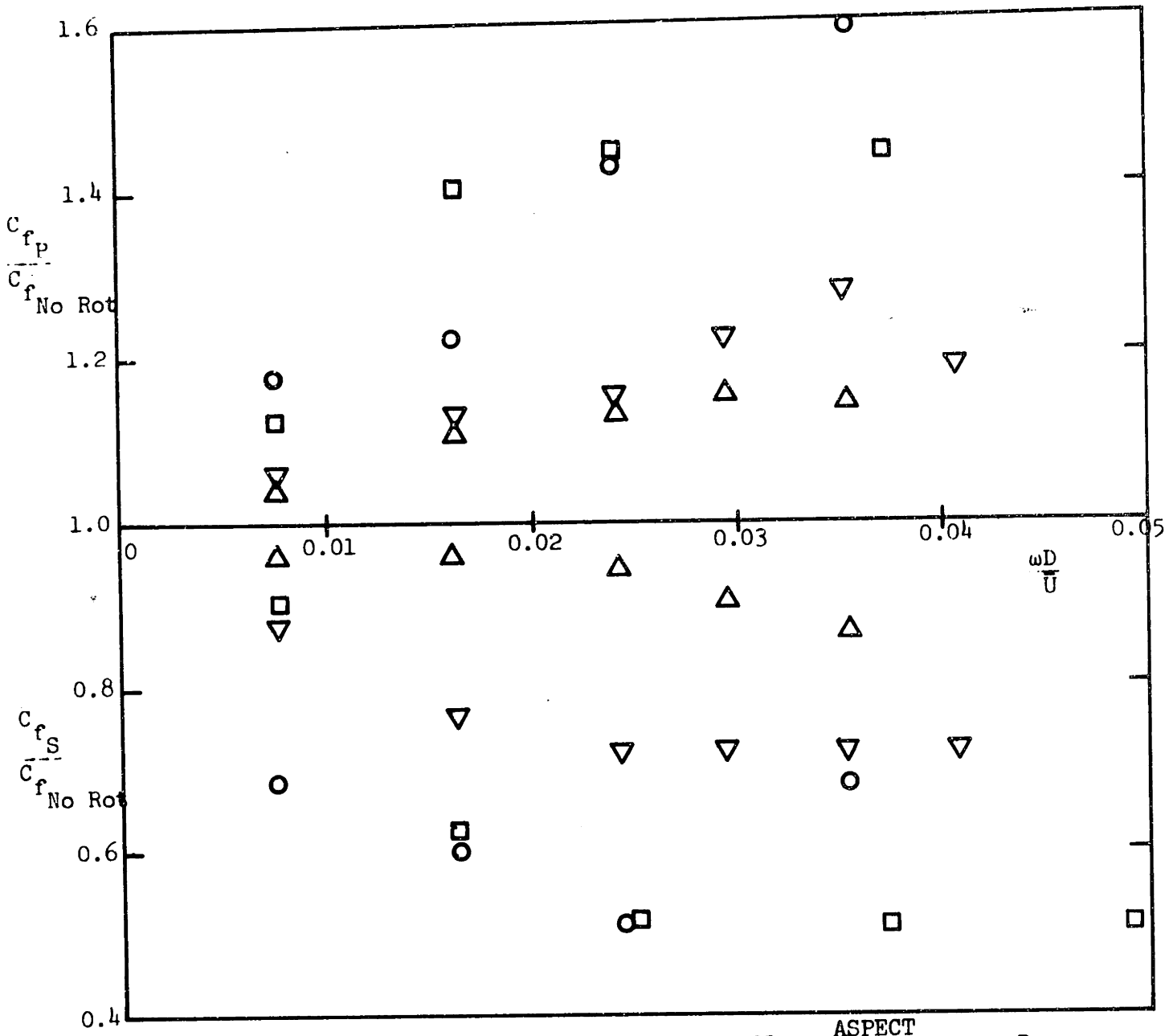

SYMBOL	ASPECT RATIO	Re_L
□	$\frac{1}{2}$: 1	2.80×10^4
○	1 : 1	1.29×10^4
▽	4 : 1	2.04×10^4
△	$7\frac{1}{3}$: 1	2.24×10^4

FIGURE 17 CENTERLINE WALL SHEAP STRESSES

$$C_f = \frac{2\tau_o}{\rho U^2}$$

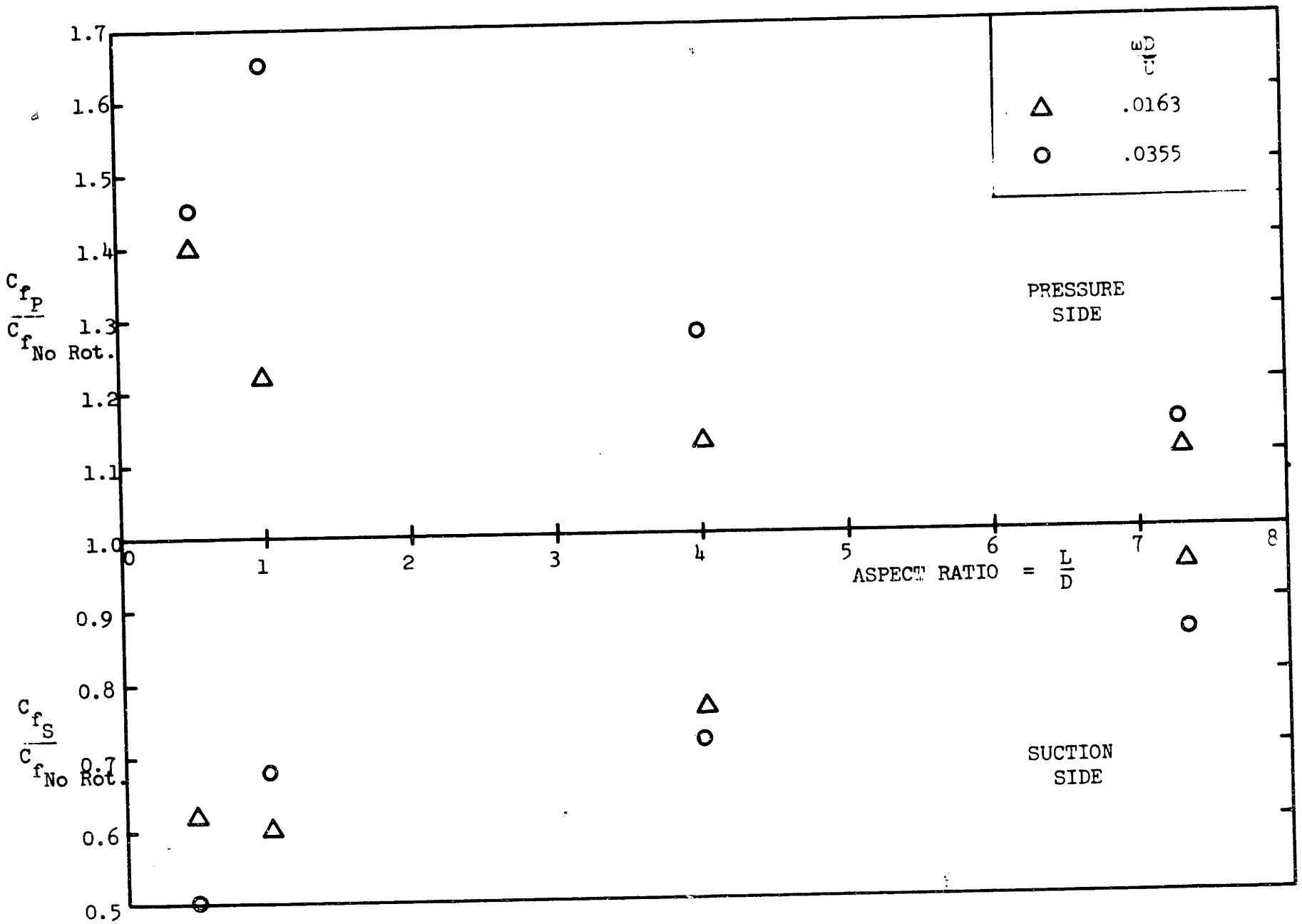

FIGURE 18 SKIN FRICTION VARIATION WITH ASPECT RATIO

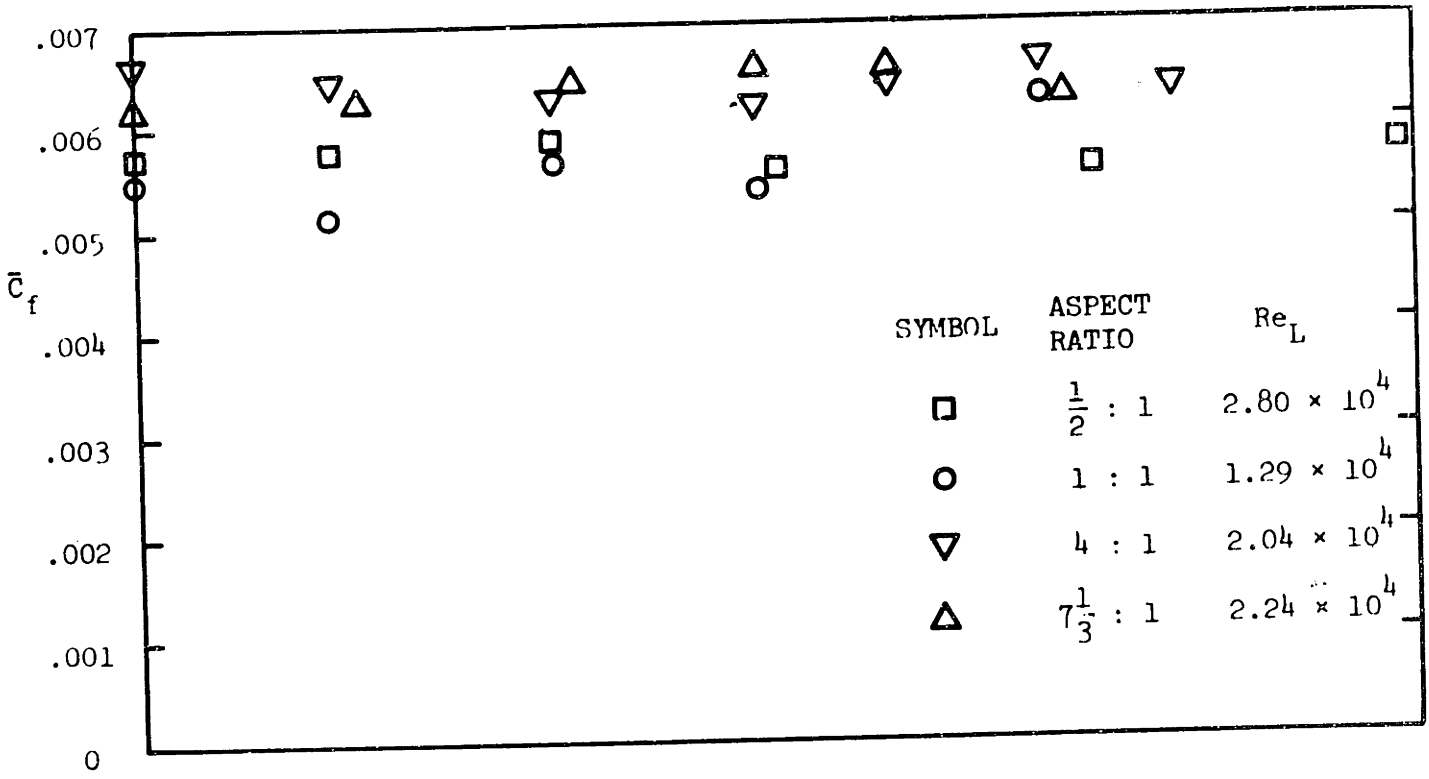

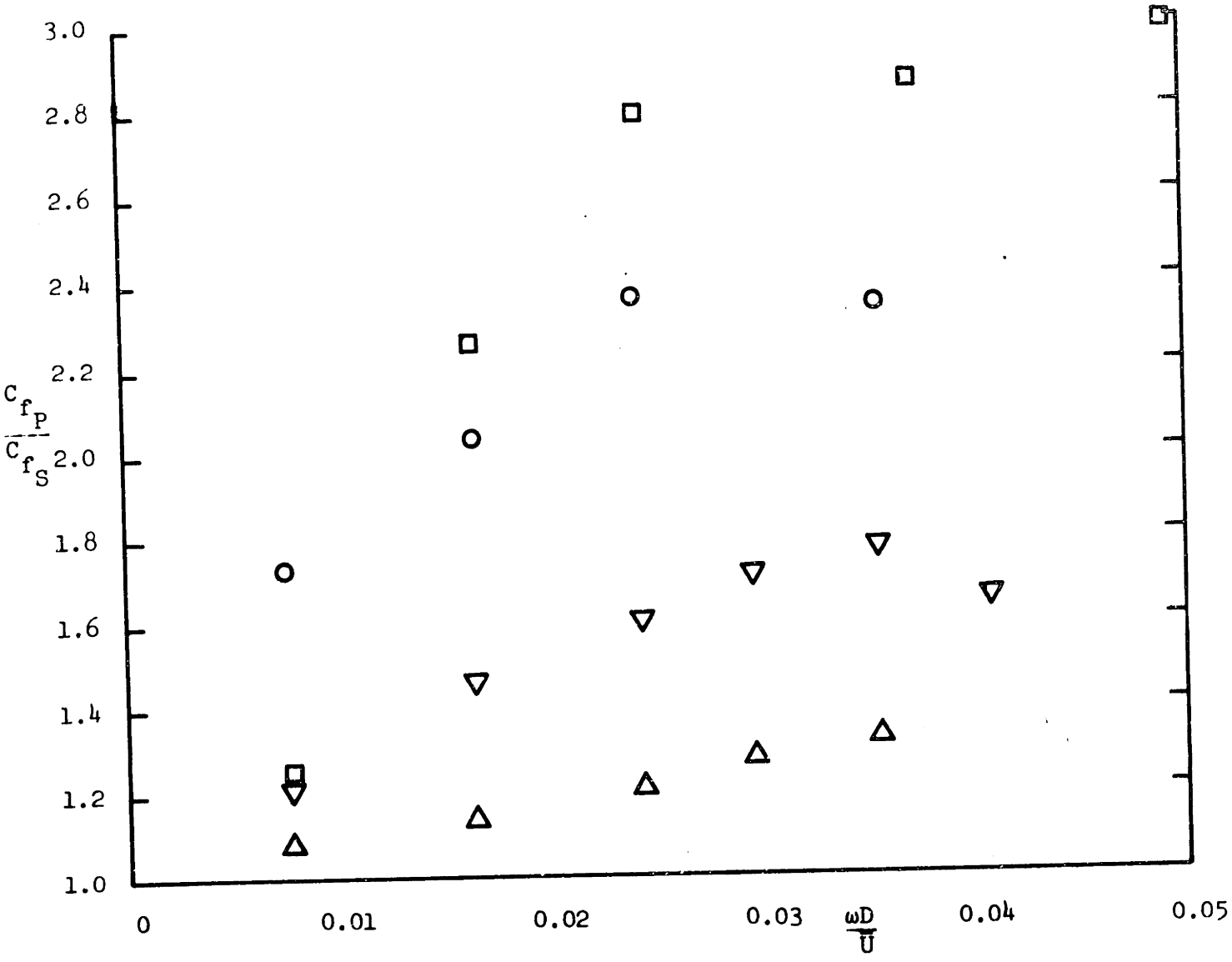

FIGURE 19 MEAN AND RATIO OF CENTERLINE WALL SHEAR STRESSES

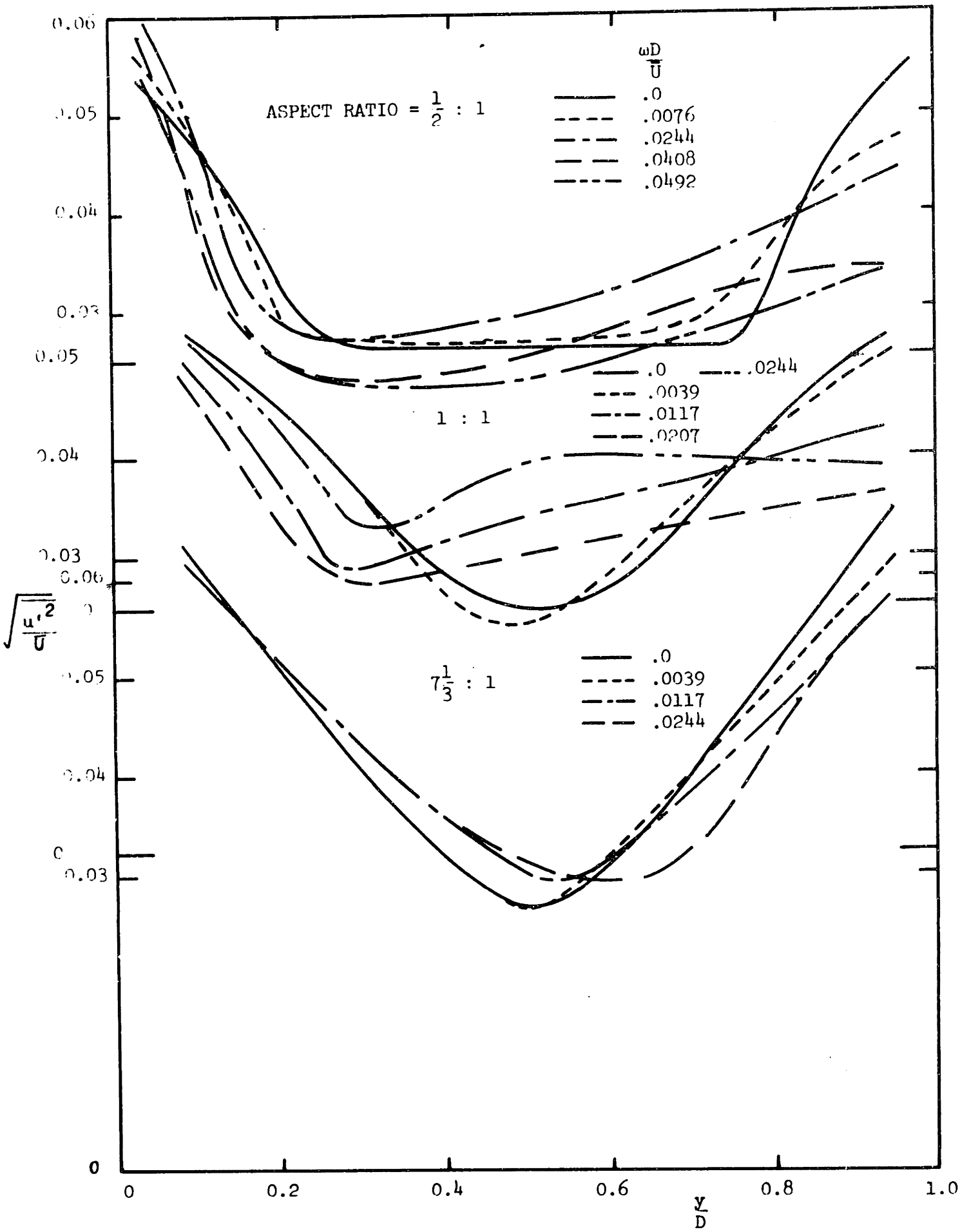

FIGURE 20 u' TURBULENCE INTENSITIES

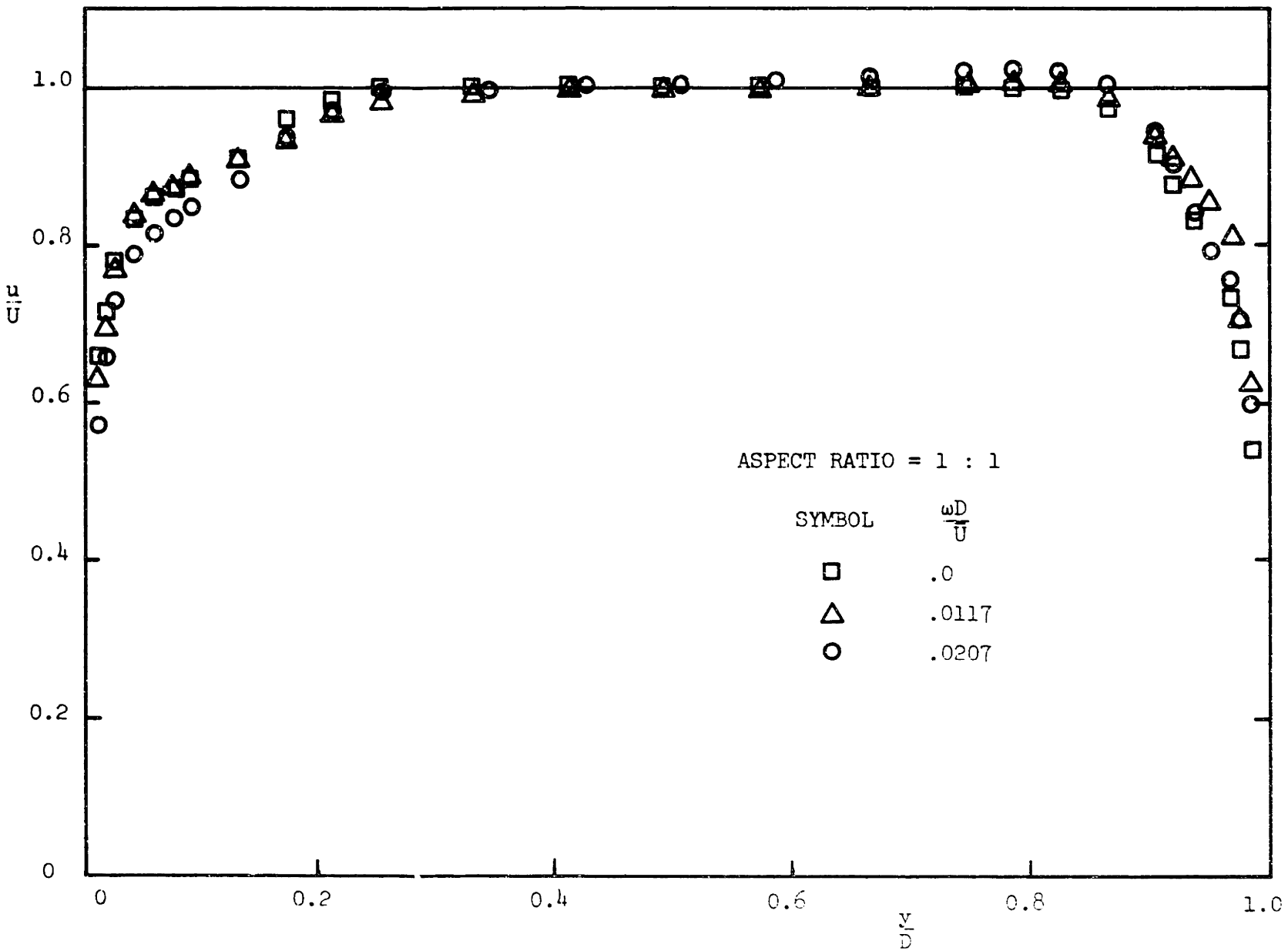

FIGURE 21 DUCT INLET VELOCITY PROFILES

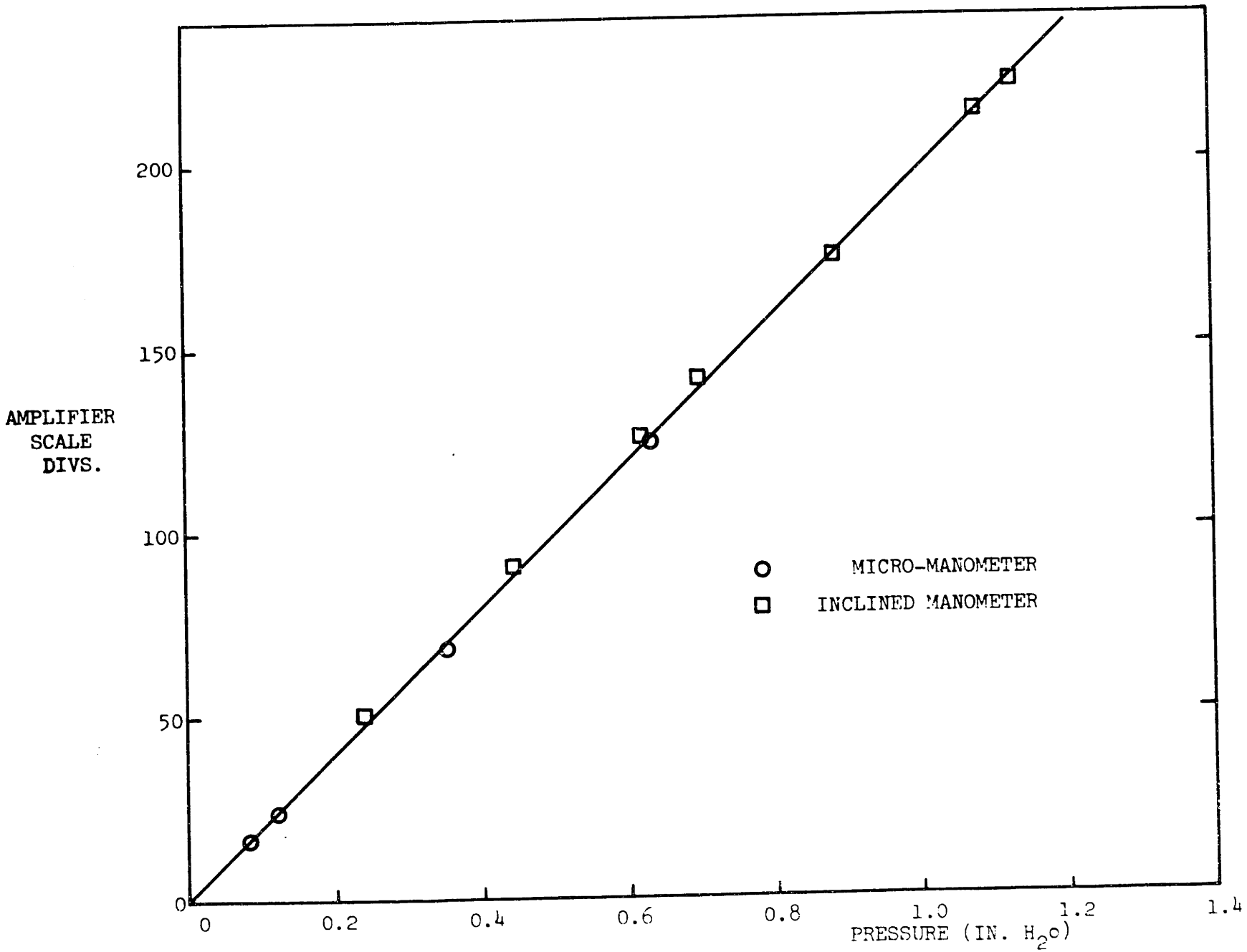

FIGURE 22 TRANSDUCER CALIBRATION CURVE

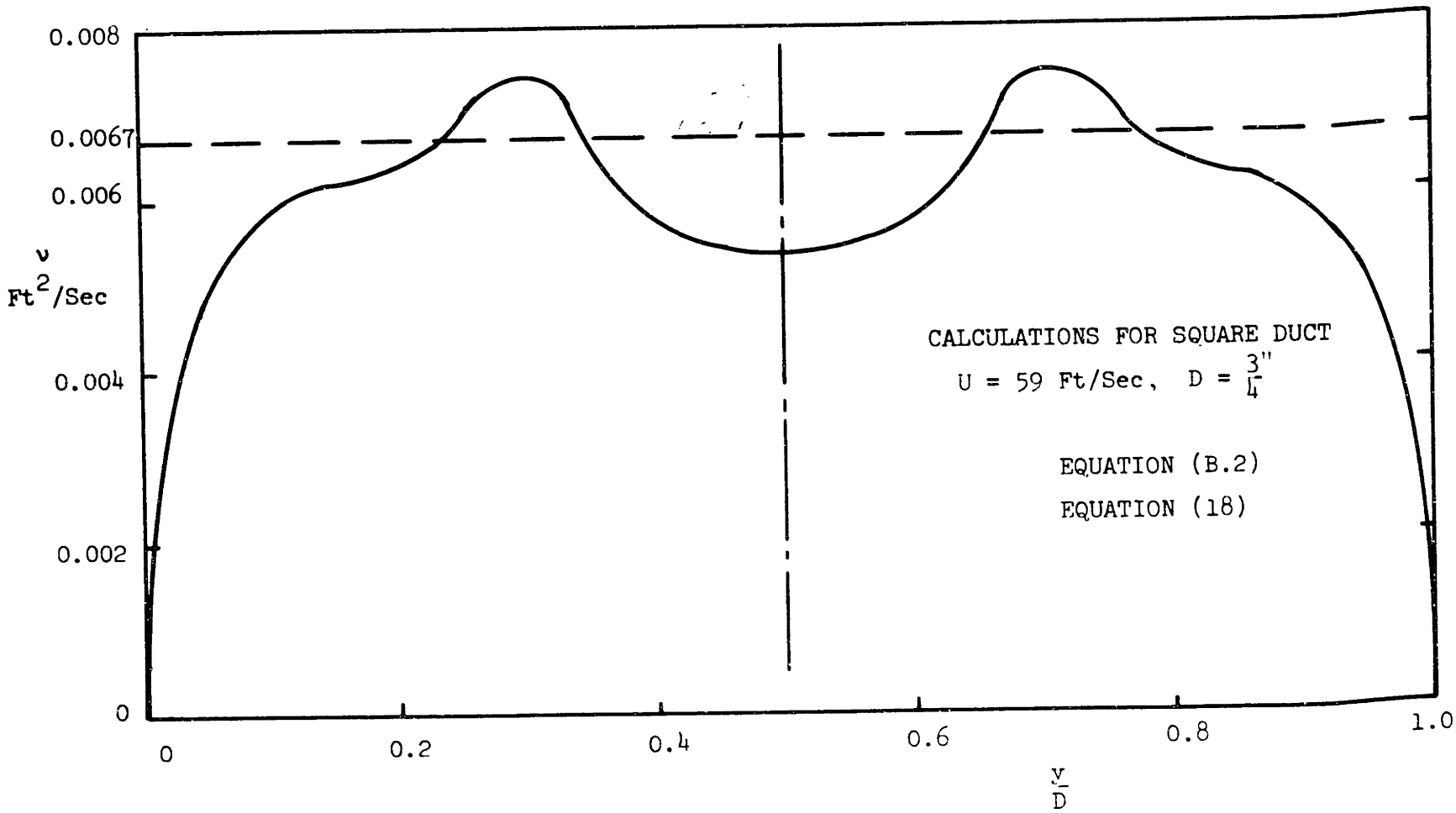

FIGURE 23 COMPARISON OF ESTIMATES OF EDDY VISCOSITY

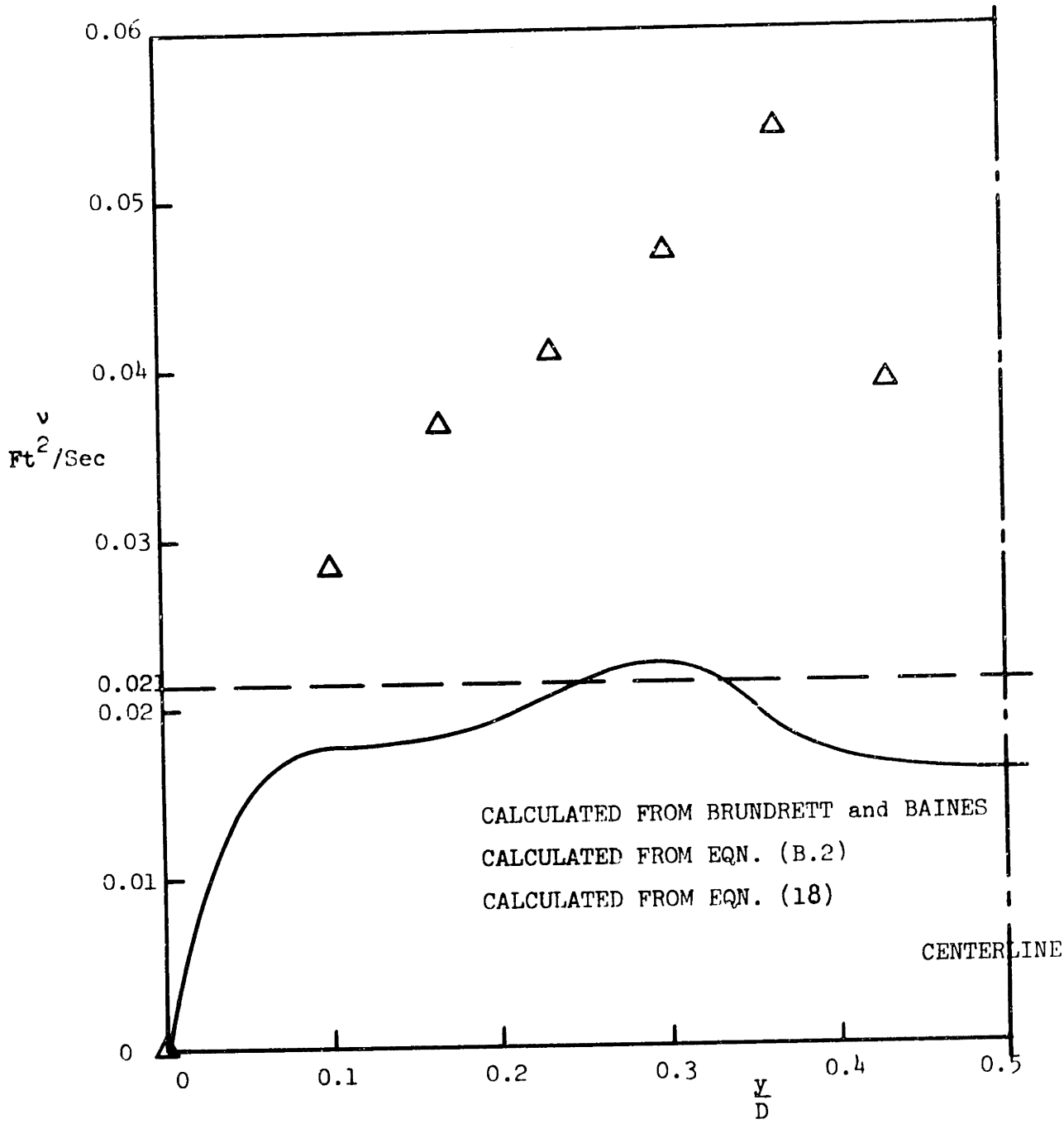

FIGURE 24 COMPARISON OF MEASURED AND CALCULATED EDDY VISCOSITY DISTRIBUTIONS FOR 3" SQUARE DUCT

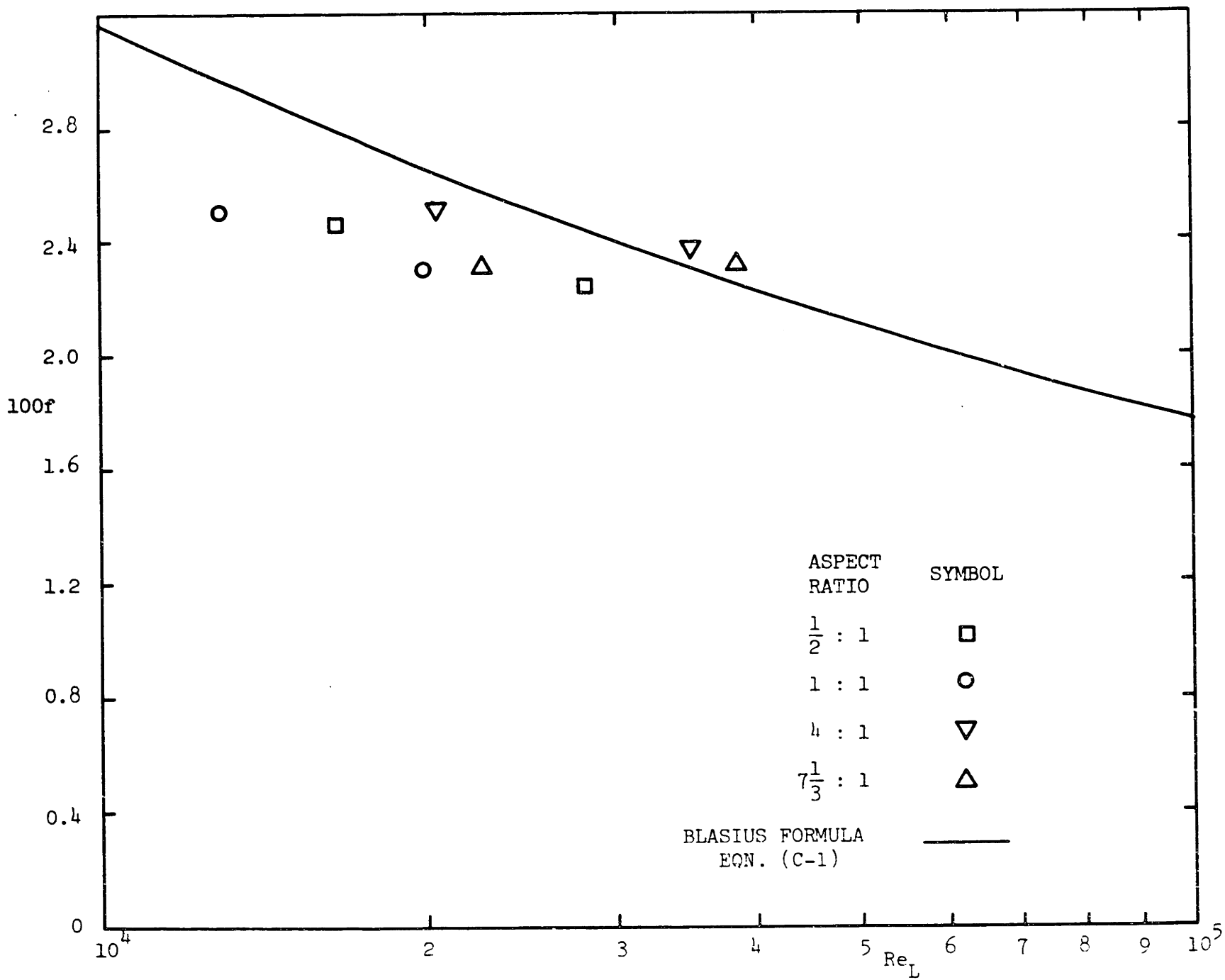

FIGURE 25 FRICTION FACTORS WITH NO ROTATION

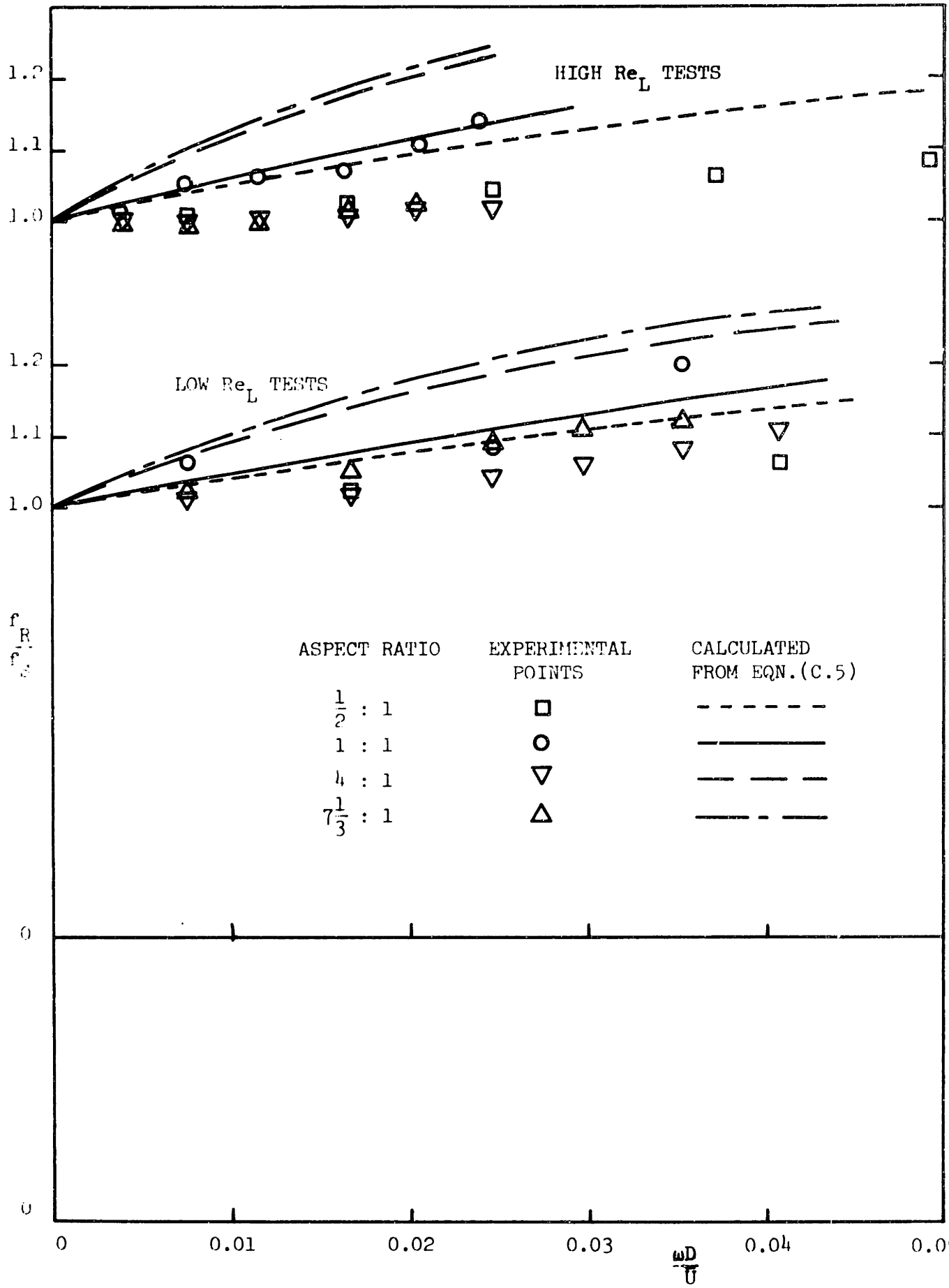

FIGURE 26 EFFECTS OF ROTATION ON FRICTION FACTOR

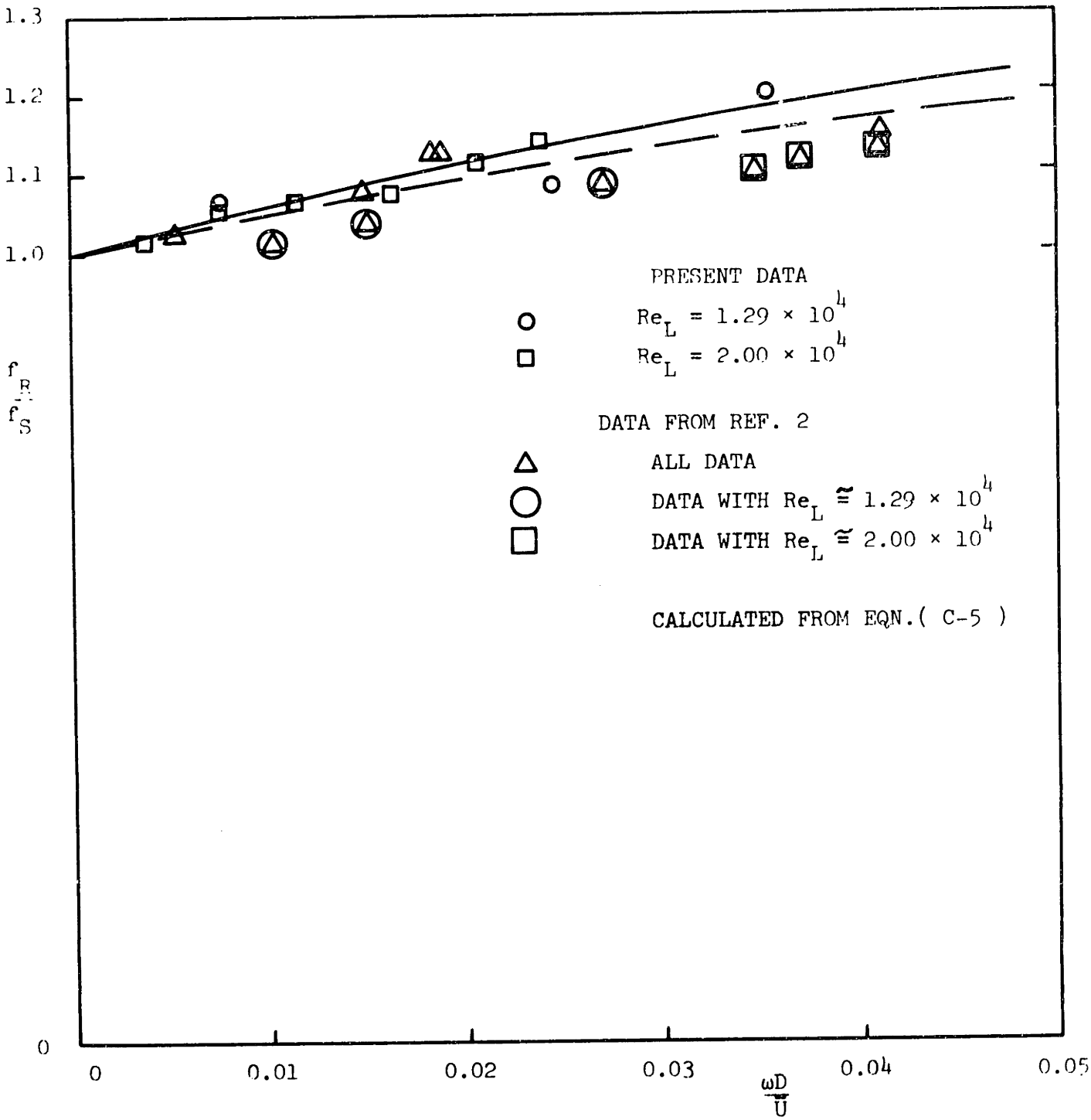

FIGURE 27 COMPARISON OF SQUARE AND CIRCULAR CHANNEL DATA FOR FRICTION FACTOR